Theoretical and Applied Climatology (2019) 135:1559–1581
https://doi.org/10.1007/s00704-018-2432-6

ORIGINAL PAPER

Aspect of ECMWF downscaled Regional Climate Modeling in simulating Indian summer monsoon rainfall and dependencies on lateral boundary conditions

Soumik Ghosh[1] · R. Bhatla[1,2] · R. K. Mall[2,3] · Prashant K. Srivastava[2,3] · A. K. Sahai[4,5]

Received: 28 February 2017 / Accepted: 19 February 2018 / Published online: 22 March 2018

Abstract

Climate model faces considerable difficulties in simulating the rainfall characteristics of southwest summer monsoon. In this study, the dynamical downscaling of European Centre for Medium-Range Weather Forecast's (ECMWF's) ERA-Interim (EIN15) has been utilized for the simulation of Indian summer monsoon (ISM) through the Regional Climate Model version 4.3 (RegCM-4.3) over the South Asia Co-Ordinated Regional Climate Downscaling EXperiment (CORDEX) domain. The complexities of model simulation over a particular terrain are generally influenced by factors such as complex topography, coastal boundary, and lack of unbiased initial and lateral boundary conditions. In order to overcome some of these limitations, the RegCM-4.3 is employed for simulating the rainfall characteristics over the complex topographical conditions. For reliable rainfall simulation, implementations of numerous lower boundary conditions are forced in the RegCM-4.3 with specific horizontal grid resolution of 50 km over South Asia CORDEX domain. The analysis is considered for 30 years of climatological simulation of rainfall, outgoing longwave radiation (OLR), mean sea level pressure (MSLP), and wind with different vertical levels over the specified region. The dependency of model simulation with the forcing of EIN15 initial and lateral boundary conditions is used to understand the impact of simulated rainfall characteristics during different phases of summer monsoon. The results obtained from this study are used to evaluate the activity of initial conditions of zonal wind circulation speed, which causes an increase in the uncertainty of regional model output over the region under investigation. Further, the results showed that the EIN15 zonal wind circulation lacks sufficient speed over the specified region in a particular time, which was carried forward by the RegCM output and leads to a disrupted regional simulation in the climate model.

Keywords ECMWF · Regional climate model · Dynamical downscaling · Summer monsoon · Boundary condition · CORDEX

Key Points
1. Assessment of sensitivity of RegCM's Mix99 (Grell -> Land & Emanuel -> Ocean) Convective Parameterization Scheme (CPS) in simulating Intraseasonal variability of Indian summer monsoon (ISM).
2. Evaluation of mixed CPS and its dependencies on boundary conditions.
3. Low efficiency of in situ lateral boundary conditions over the particular region causes a disturbed rainfall characteristic in RegCM simulation.
4. Low efficiency in EIN15 zonal wind circulation over Indian region during the phases of monsoon.

✉ R. Bhatla
rbhatla@bhu.ac.in

[1] Department of Geophysics, Institute of Science, Banaras Hindu University, Varanasi, India

[2] DST-Mahamana Centre of Excellence for Climate Change Research, Institute of Environment & Sustainable Development, Banaras Hindu University, Varanasi, India

[3] Institute of Environment and Sustainable Development, Banaras Hindu University, Varanasi, India

[4] Indian Institute of Tropical Meteorology, Pune, Maharashtra, India

[5] India Meteorological Department, Pune, India

Abbreviations

BATS	Biosphere-Atmosphere Transfer Scheme
BoB	Bay of Bengal
CCSM3	Community Climate System Model version 3
CLM	Climate Local Model
CMO	Conditional model output
CORDEX	Co-Ordinated Regional Climate Downscaling EXperiment
COSMO	Consortium for Small-Scale Modeling
CPS	Convective Parameterization Scheme
ECDF	Empirical cumulative distribution function
ECHAM5	Fifth-generation atmospheric GCM developed at the Max Planck Institute for Meteorology
ECMWF	European Centre for Medium-Range Weather Forecasts
EIN15	ERA-Interim
ERSST	Extended Reconstructed Sea Surface Temperature
GCM	Global climate model
hPa	Hectopascal
ICBC	Initial condition and boundary condition
ICTP	International Center for Theoretical Physics
IMD	India Meteorological Department
ISM	Indian summer monsoon
ISMR	Indian summer monsoon rainfall
LLJ	Low-level jet
MM5	Mesoscale model version 5
MPIOM	Max Planck Institute Ocean Model
MSLP	Mean sea level pressure
NCAR	National Center for Atmospheric Research
NCDC	National Climate Data Center
NOAA	National Oceanic and Atmospheric Administration
OI_WK	OISST in weekly pattern
OISST	Optimum Interpolation Sea Surface Temperature
OLR	Outgoing Longwave Radiation
Q-Q	Quantile–quantile
RCM	Regional Climate Model
RegCM	RCM by ICTP
SD	Standard deviation
SST	Sea Surface Temperature

1 Introduction

One of the most important features of global atmospheric circulation is the Indian summer monsoon (ISM) (Webster et al. 1998). Any alteration in this circulation causes a direct impact on the developing country like India, where 60% of agriculture depends only on the seasonal monsoonal rainfall (Central Statistical Organization 1998). For understanding this, many studies have been conducted in the past and well documented in the technical literature domain by using the state of the art Regional Climate Model (RCM) (Bhatla et al. 2016; Singh et al. 2017) and Global Climate Model (GCM) (ParthSarthi et al. 2016, 2015).

The RCM and GCM are the two widely used tools, which are generally used to simulate climate circulation processes and understanding the system. In recent decade, a number of studies have been conducted to simulate the ISM variability by using the RegCM (Bhatla et al. 2016; Maharana and Dimri 2016; Dash et al. 2015; Raju et al. 2015; Sinha et al. 2013; Maurya et al. 2017; Dobler and Ahrens 2010). However, the use of high-resolution RegCM in simulation of intraseasonal monsoon variability and its different epochs is still limited in the literature. In the last decade, several studies have been conducted with downscaled global reanalysis datasets from RegCM over particular boundaries (Bhatla et al. 2016; Dobler and Ahrens 2010; Saeed et al. 2009; Dash et al. 2015; VenkataRatnam and Kumar 2005; Park and Hong 2004). In the sensitivity analysis by Dash et al. (2006) and Bhatla and Ghosh (2015), the authors have found that the Grell CPS is performing better than the other CPSs in simulations of rainfall distribution by RegCM. Bhatla et al. (2016) have shown the performance of CPSs in the RegCM-4.3 over Indian land-sea continental margin and found that the Tiedtke CPS is highly efficient when compared with the in situ observations. Dobler and Ahrens (2010) have considered the RegCM simulations with the Consortium for Small-Scale Modeling (COSMO) CLM RegCM over South Asia by using the input data from ECHAM5–MPIOM and a 45-year re-analysis of European Centre for Medium-Range Weather Forecasts (ECMWF). The study showed that the mean variability of monsoon indices improves when simulated using the COSMO RegCM and compared against the driving field of ECHAM5–MPIOM. With the use of GCM downscaled output at regional level (Almazroui 2016, 2012; Saeed et al. 2009), Tugba et al. (2016) simulated the seasonal rainfall with the RegCM-4.3.5 over Central Asia. All the above studies showed a better performance of the RCM by capturing the regional phenomena, although it varies depending on the seasons, parameterization schemes along with some biases, and the role of initial condition. Singh et al. (2017) suggested a proper evaluation of RCM model output and its utilization in further climate studies by highlighting the poorer simulation of GCM downscaled output than the respective GCM simulations. According to them, most of RCMs have not added any significant output for the past, present, and future time scales in simulating Indian summer monsoon rainfall (ISMR) behavior as compared to the GCMs. Most of the studies have raised questions in RCM's performance by considering various initial condition and boundary condition (ICBC) for climate modeling study (Mishra et al. 2014; Singh et al. 2017; Dash et al. 2015) rather than cross verifying the host GCM simulations and finding out the authenticity of the RCM's ICBC.

In purview of the above, this study aims to improve the simulation of the dynamical mechanism of ISM by using the time-dependent ECMWF ICBC, through the RegCM-4.3 model downscaling along with the various sea surface temperature (SST) specified over the ocean. Further, through this study, an attempt has been made to understand the dependencies of model simulation with ERA-Interim (EIN15) ICBC and deducing its impact on the model simulated rainfall over a particular region during the phases of ISM rainfall.

2 Data and methodology

2.1 RegCM-4.3 outline

The conceptual innovation of the RegCM was originally developed in the late 1980s from the National Center for Atmospheric Research (NCAR), USA. With the core of MM4 (Grell et al. 1994), Giorgi and Bates (1989) and Dickinson et al. (1989) introduced the first version of RegCM model in 1989. After several upgrades in model physics, RegCM-3 was introduced in which model grid spacing was extended between 10 and 100 km with simultaneous ranging from seasonal to centennial periods covering all land regions over the world (except Polar region). This version of RegCM was more portable and developed with an aim to simulate the tropical climates (Giorgi and Anyah 2012). The RegCM-4 is then upgraded with integration of new land surface physics, planetary boundary layer conditions and air–sea flux scheme. With the modification in pre-existing radiative transfer and boundary layer schemes, the mixed convection scheme was developed and the model code was upgraded to improve its flexibility and applicability (Giorgi et al. 2012).

The RegCM-4.3 is a hydrostatic model with sigma-p vertical coordinate system and having capability to run over a large range of Regional Climate Modeling system (Giorgi et al. 2012). It is the first limited area model with the mesoscale model version 5 (MM5) dynamical core, developed by the International Center for Theoretical Physics (ICTP) for a long-range climate simulation running on Arakawa B-grid. In this version, two types of land-use (BATS) have been added for the better representation of the urban and suburban environments. For urban development, the surface albedo has been modified and the surface energy balance is modified for alter. The Climate Local Model (CLM) version 3.5 is coupled with the RegCM-4.3, which deals with the bio-geophysical-based parameterization and to describe the exchanges of energy, momentum, water, and carbon (Tawfik and Steiner 2011) along with the physical process given by Holtslag et al. (1990) for the planetary boundary layer (PBL). The RegCM-4.3 has four core CPSs: Grell (Grell 1993), Emanuel (Emanuel 1991; Emanuel and Živković-Rothman 1999), Tiedtke, and Kuo. The Arakawa–Schubert or the Fritsch and Chappell (1980a, 1980b) type closures are available to use with the Grell CPS. It has the capacity to perform combinations of different CPSs over the land and ocean. The RegCM-4.3 has been forced to simulate the mixed convection scheme mode: Mix98 (Grell over the ocean, Emanuel over the land) and Mix99 (Grell over the land, Emanuel over the ocean). The lower boundary conditions are derived from six hourly forcing of EIN15 re-analysis. These ICBCs are obtained with the 1.5° horizontal grids and 37 vertical levels, which incorporate the CCSM3 radiation scheme of NCAR Community (Kiehl et al. 1996; Collins et al. 2006). The CPSs are forced with the Optimum Interpolation Sea Surface Temperature (OISST) in weekly pattern (OI_WK) and Extended Reconstructed Sea Surface Temperature (ERSST) wherever applicable. The dataset of OI_WK at weekly and ERSST at six hourly timescales are obtained from the National Oceanic and Atmospheric Administration (NOAA) and National Climate Data Center (NCDC), respectively. The details of the RegCM-4.3 configuration are listed in Table 1.

2.2 Experiment design

The complicated characteristic of South Asian summer monsoon rainfall faces considerable difficulty in rainfall simulation over the region (Webster et al. 1998). Dealing with the complex topography and coastline terrain, the RegCM is equipped with advance numerical and physical schemes (Giorgi et al. 2001). With the flexibility in choosing the appropriate CPS over a particular domain, this study is continued with Mix99 CPS. Several studies have showed the better performance of Grell CPS over the land region (Bhatla and Ghosh 2015; Elguindi et al. 2013) and produced good simulation of Emanuel CPS over the ocean. The combination of core CPSs (Grell and Emanuel) with their better side is termed as Mix99 scheme, where Grell CPS is used over the Land and Emanuel over the ocean. The variation in mean seasonal rainfall has a strong association with the global phenomena through the influence of SST (Krishnamurthy and Kinter 2003). Therefore, for sensitivity analysis, the conditional model outputs (CMOs) are continued with two types SST (ERSST and OI_WK) as lower boundary conditions. For better representation in response to climate dynamics, associations with atmospheric convection and topographical complexity have been conducted at 0.5° × 0.5° fine resolution through the model simulation. For this synoptic study, the model simulated daily rainfall, Outgoing Longwave Radiation (OLR), mean sea level pressure (MSLP) and wind at 925 hPa and 850 hPa vertical pressure intervals over the South Asia CORDEX region (22°S-50°N and 10°E-130°E). The actual onset dates (Table 2) are considered as per the India Meteorological Department (IMD) guidelines, while the active/break spells are obtained from the NCC Research Report (2013) provided by the IMD (Table 3). 30 years

Table 1 Model configuration of the RegCM4.3

Dynamics	Hydrostatics
Model domain	South Asia CORDEX domain (15°S–45°N; 10°E–130°E)
Domain cartographic projection	ROTMER—rotated Mercator
Resolution	50 km horizontal
Vertical level	18 sigma vertical levels
Initial and boundary conditions	ERA15
SST	1. OI_WK – OISST weekly optimal interpolation dataset 2. ERSST – ERA-Interim 6 hourly 1.5°×1.5° SST
Land surface parameterization Radiation	Modified CCM3
Parameterization PBL	Modified Holtslag
Convective parameterization	Mix99 (Emanuel over the ocean and Grell over the land)
Grell closure scheme	Arakawa and Schubert (1974)

(1981–2010) climatological composites of the considered parameters are analyzed to find out the predictive skills. Maharana and Dimri (2016) have illustrated the simulation process and the physics of the RegCM, which plays a dominant role in defining the intraseasonal variability. But the model simulation is not well correlated with the in situ observations obtained during the intraseasonal/interannual rainfall simulations, and the correlation coefficient is found close to zero (Maharana and Dimri 2014, 2016). Therefore, the correlation coefficient has not been considered as a verification tool for different CMOs with the in situ observations. In this study, the performance verification between in situ and the model derived outputs is verified using quantile–quantile (Q-Q) distribution, empirical cumulative distribution function (ECDF), SD, and absolute bias (bias) for different phases of summer monsoon. The bias can be measured as follows:

$$\text{Bias} = \left[\left(\overline{y}-\overline{x}\right)\right]$$

where the optimal value is 0 and the low magnitude value indicates high accuracy in model simulation. $\overline{x}$ represents the mean of the observed/reanalyzed data and $\overline{y}$ is the mean of the model output.

3 Results and discussion

3.1 Variability of summer monsoon with different lower boundary conditions

3.1.1 Onset phase

In order to simulate the summer monsoon rainfall variability, the ICBC ERSST and OI_WK SST forcing are considered. Spatial distributions of CMOs and in situ datasets for different phases of summer monsoon are provided in Figs. 1 to 3. Due

Table 2 Actual and model simulation onset dates along with their deviation from actual onset of ISM with different initial condition

	Onset dates		
Year	Actual	OI_WK	ERSST
1981	30 M	–	24 M (− 6)
1982	28 M	04 J (+ 7)	02 J (+ 5)
1983	13 J	21 J (+ 8)	21 J (+ 8)
1984	30 M	31 M (+ 1)	31 M (+ 1)
1985	28 M	29 M (+ 1)	06 J (+ 9)
1986	04 J	25 M (− 10)	24 M (− 11)
1987	02 J	08 J (+ 6)	07 J (+ 5)
1988	26 M	23 M (− 3)	27 M (+ 1)
1989	03 J	25 M (− 9)	29 M (− 5)
1990	19 M	19 M (0)	18 M (− 1)
1991	02 J	07 J (+ 5)	02 J (0)
1992	05 J	06 J (+ 1)	25 M (− 11)
1993	28 M	30 M (+ 2)	31 M (+ 3)
1994	28 M	06 J (+ 9)	04 J (+ 7)
1995	05 J	11 J (+ 6)	11 J (+ 6)
1996	03 J	24 M (− 10)	03 J (0)
1997	09 J	–	29 M (− 11)
1998	02 J	30 M (− 3)	30 M (− 3)
1999	25 M	02 J (+ 8)	21 M (− 4)
2000	01 J	25 M (− 7)	–
2001	23 M	26 M (+ 3)	22 M (− 1)
2002	29 M	17 M (− 12)	17 M (− 12)
2003	08 J	06 J (− 2)	–
2004	18 M	21 M (+ 3)	12 M (− 6)
2005	05 J	07 J (+ 2)	09 J (+ 4)
2006	26 M	25 M (− 1)	28 M (+ 2)
2007	28 M	–	01 J (+ 4)
2008	31 M	31 M (0)	26 M (− 5)
2009	23 M	–	–
2010	31 M	19 M (− 12)	21 M (− 10)

Where *M* May and *J* June

Table 3 Active/break periods and days of summer monsoon during 1981–2010

Year	Active spells	Break spells	No. of active/break spells	No. of active/break days
1981	7–10 J	24–27 A	Act = 1, brk = 1	Act = 5, brk = 4
1982	21–23 A, 12–14 A	1–8 J	Act = 2, brk = 1	Act = 6, brk = 8
1983	18–20 A	14–16 J	Act = 1, brk = 1	Act = 3, brk = 3
1984	1–3 A, 9–11 A, 16–19 A	28–30 J	Act = 3, brk = 1	Act = 10, brk = 3
1985	15–17 J, 30 J–2 A, 6–8 A	23–25 A	Act = 3, brk = 1	Act = 10, brk = 3
1986	21–24 J, 13–15 A	23–31 A	Act = 2, brk = 1	Act = 7, brk = 9
1987	24–29 A	23–25 J, 30 J–4 A, 9–13 A	Act = 1, brk = 3	Act = 6, brk = 14
1988	26–28 J	14–17 A	Act = 1, brk = 1	Act = 3, brk = 4
1989	–	18–20 J, 30 J–3 A	Act = 0, brk = 2	Act = 0, brk = 8
1990	2–4 J, 21–24 A, 29–31 A	–	Act = 3, brk = 0	Act = 10, brk = 0
1991	21–24 J, 29–31 J, 22–24 A	1-3 J	Act = 3, brk = 1	Act = 10, brk = 3
1992	27–29 J, 16–21 A	4–10 J	Act = 2, brk = 1	Act = 9, brk = 7
1993	7–11 J, 15–17 J	20–23 J, 8–13 A, 22–28 A	Act = 2, brk = 3	Act = 8, brk = 17
1994	2–4 J, 9–16 J, 30 J–2 A, 18–20 A, 25–27 A, 29–31 A	–	Act = 6, brk = 0	Act = 24, brk = 0
1995	18–20 J, 22–25 J	3–7 J, 11–17 A	Act = 2, brk = 2	Act = 7, brk = 12
1996	24–28 J, 19–21 A	11–13 A	Act = 2, brk = 1	Act = 8, brk = 3
1997	30 J–1 A, 21–25 A	11–15 J, 9–17 A	Act = 2, brk = 2	Act = 8, brk = 14
1998	30 J–1 A, 21–25 A	21–26 J, 16–21 A	Act = 2, brk = 2	Act = 8, brk = 12
1999	7–9 A	1–5 J, 12–18 A, 22–24 A	Act = 1, brk = 3	Act = 3, brk = 15
2000	12–14 J, 17–20 J	29 J–8 A	Act = 2, brk = 1	Act = 7, brk = 11
2001	9–12 J	31 J–2 A, 27–29 A	Act = 1, brk = 2	Act = 4, brk = 6
2002	23–25 A	4–16 J, 22–31 J	Act = 1, brk = 2	Act = 3,brk = 23
2003	23–28 J, 27–29 A	–	Act = 2, brk = 0	Act = 9, brk = 0
2004	8–13 A, 21–23 A	10–13 J, 19–22 J, 26–31 A	Act = 2, brk = 3	Act = 9, brk = 14
2005	1-5 J, 25–29 J, 31 J–2 A	7–14 A, 24–31 A	Act = 3, brk = 2	Act = 13, brk = 16
2006	3–6 J, 27 J–7 A, 13–15 A, 17–20 A	–	Act = 4, brk = 0	Act = 23, brk = 0
2007	1–9 J, 6–9 A	18–23 J, 15–17 A	Act = 2, brk = 2	Act = 13, brk = 9
2008	10–12 A	16–21 J, 21–24 A, 28–30 A	Act = 1, brk = 3	Act = 3, brk = 13
2009	13–16 J, 20–23 J	29 J–9 A, 17–19 A	Act = 2, brk = 2	Act = 8, brk = 15
2010	–	–	Act = 0, brk = 0	Act = 0, brk = 0
Total (1981–2010)	No. of spells: Act = 59, brk = 44	No. of days: Act = 237, brk = 246		

J July, *A* August, *act* active, *brk* break

to unavailability of regular time period of SST, the data length for in situ and CMO ERSST are considered only for the period 1981–2010, while for CMO OI_WK runs are provided for the time period 1982–2010. The rainfall and OLR distribution during the onset phase of summer monsoon rainfall are represented through Fig. 1a–f. For simulating the onset phase, IMD onset simulation criteria (Pai and Rajeevan 2007) are considered. The onset criterion is emphasized by using the peak of rainfall over Kerala with four (4) newly developed conditions, which is dependent upon the three climatic parameters. Sixty percent of rainfall stations is found in the Kerala (a total of 14 stations namely Minicoy, Amini, Thiruvananthapuram, Punalur, Kollam, Allapuzha, Kottayam, Kochi, Trissur, Kozhikode, Talassery, Cannur, Kasargode, and Mangalore) with a minimum rainfall of 2.5 mm/day for the two consecutive days (after 10th of May) which is considered as the onset of monsoon. For declaration of onset, another three criteria also have to be satisfied along with the station wise rainfall criteria. The depth of westerly will have to be maintained at 600 hPa over 0°N–10°N and 55°E–80°E regions. Zonal wind will have to be blown at a speed of 15–20 knots at 925 hPa over the Lat 5°N–10°N and Lon 70°E–80°E, and INSAT OLR should be less than 200 Wm^{-2} over Lat 5°N–10°N and Lon 70°E–75°E.

High-resolution (0.25 × 0.25°) IMD rainfall data is considered for spatial and temporal rainfall analysis which is distributed only over the Indian subcontinent. Two stations (Minicoy and Amini) among the 14 stations do not have the rainfall distributed area in IMD rainfall data. Therefore, only 12 stations are considered to carry out this present study. Table 2

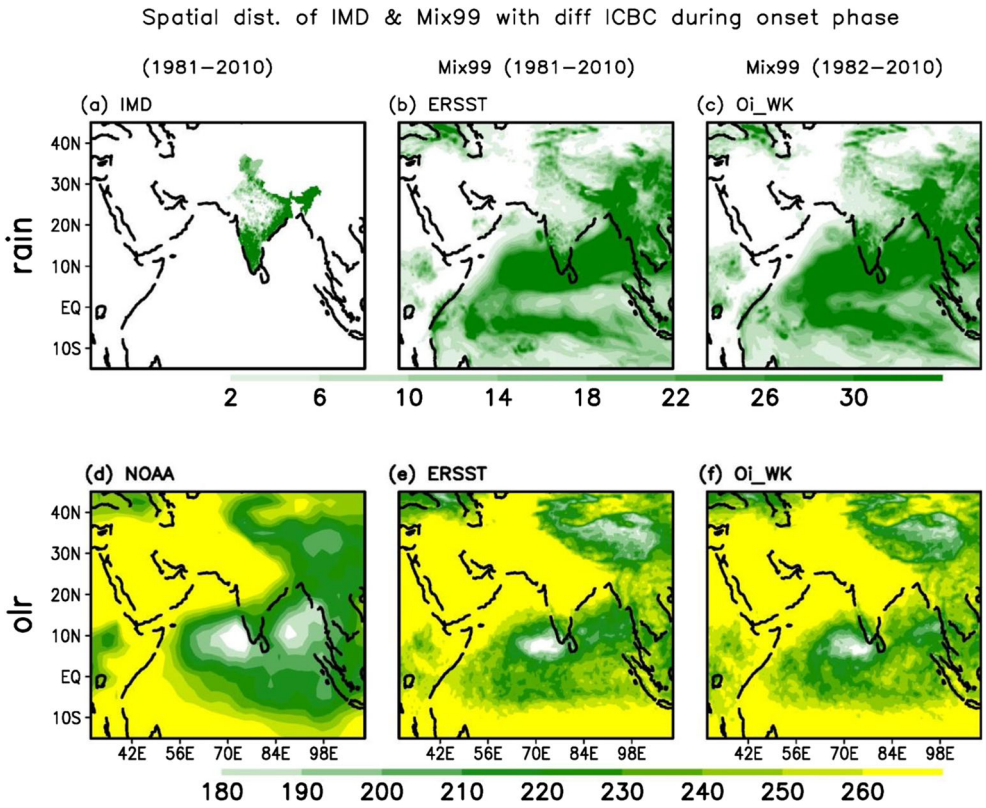

Fig. 1 **a–f** Spatial pattern of in situ and CMO-simulated rainfall and OLR distribution during 1981–2010 by following IMD criteria for declaring monsoon onset

illustrates the actual onset along with CMO onset simulation followed by IMD criteria. Some years are left blank that do not satisfy the said criteria. IMD mean rainfall distribution (Fig. 1a) during the two consecutive days (previous day of actual onset and the actual onset) showed a densely rainfall distribution over the adjoining part of the Kerala and Western Ghat region and represents 2.5 mm/day of rainfall criteria over the Kerala region. The ERSST CMO (Fig. 1b) and OI_WK CMO (Fig. 1c) are following the pattern of IMD rainfall distribution during two consecutive days of model-simulated onset. Because of unavailability of the long-range climatological INSAT OLR, in this study, the CMO OLR distribution is cross-verified by using the NOAA in situ data instead of INSAT OLR. Figure 1d represents the NOAA in situ OLR distribution where CMO ERSST and CMO OI_WK are considered and shown in Fig. 1e, f, respectively. Distributions of

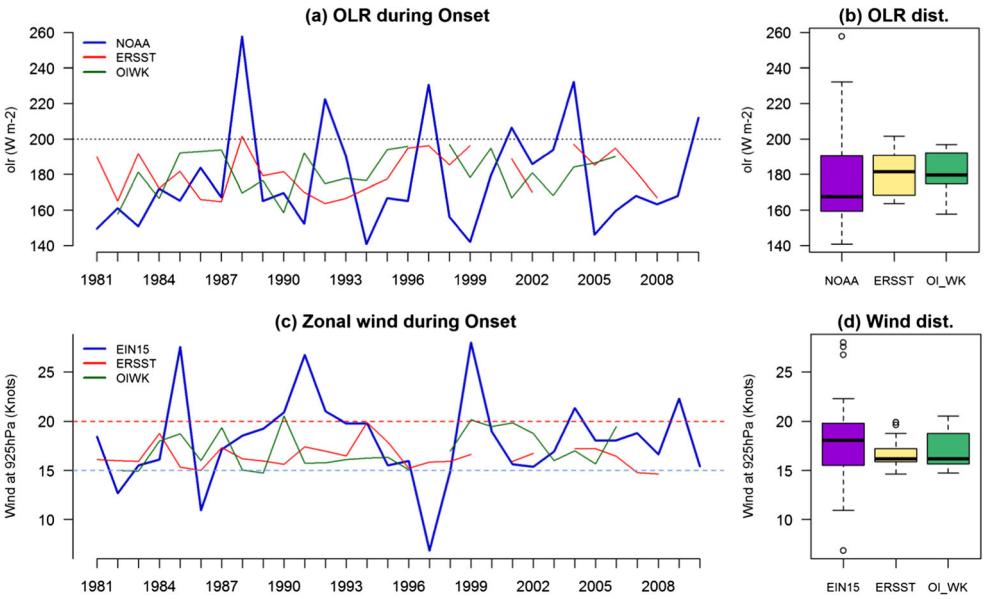

Fig. 2 **a–d** Distribution of in situ and CMOs simulation of OLR over the region Lat 5°N–10°N and Lon 70°E–75°E and zonal wind at 925 hPa over the region Lat 5°N–10°N and Lon 70°E–80°E for the respective onset date

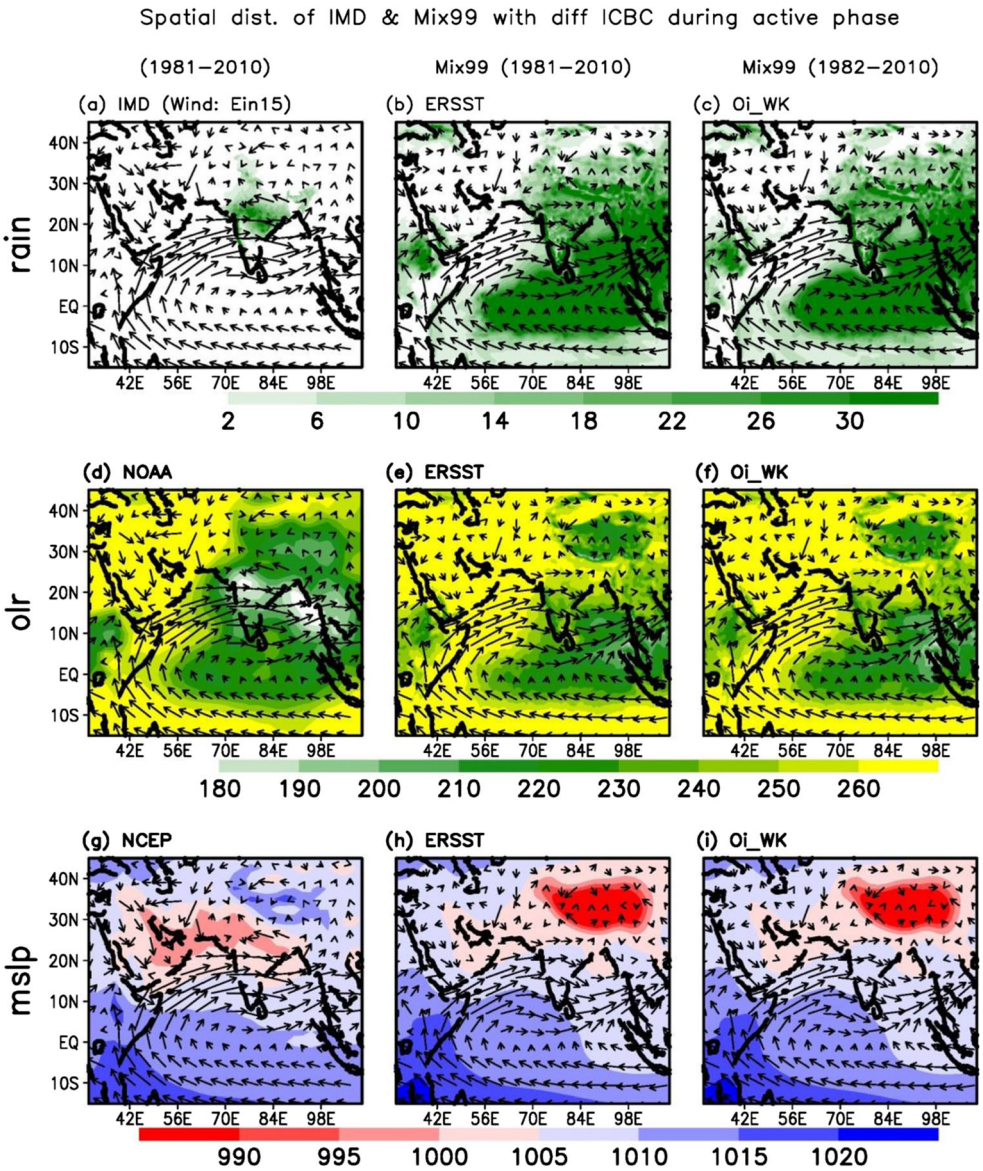

Fig. 3 **a–i** Composite spatial pattern of in situ and CMO-simulated rainfall, OLR, and MSLP distribution during active phases for duration 1981–2010. EIN15 and CMO-derived wind circulation is superimposed at 850 hPa for respective cases

CMO OLR pattern are in close match with the in situ OLR distribution and correctly following the in situ OLR distribution over Lat 5°N–10°N and Lon 70°E–75°E and satisfying the OLR distribution of less than 200 Wm^{-2} criteria. The temporal distributions of OLR over the region are also considered in Fig. 2a, which represent warm bias for some cases of NOAA OLR on actual onset date. But declaring onset over Indian region, NOAA as well as CMOs should maintain the limit of less than 200 Wm^{-2} over the respective region (IMD criteria) on the onset day. In this figure, the dotted line is indicating the limit band at 200 Wm^{-2}. But with a large variation, in situ OLR distribution (Fig. 2b) is found in between ~ 160–190 Wm^{-2}, while the 25th and 75th percentiles and its median are found towards the lower head of the inter quartile range box. Therefore, the spatial pattern of in situ OLR (Fig. 1d) represents the best fit with the IMD onset criteria. CMO ERSST and OI_WK are showing some deviations in the simulated onset dates, as shown in the box plots (Fig. 2b). Zonal wind speed at 925 hPa over Lat 5°N–10°N and Lon 70°E–80°E is considered in Fig. 2c in which red dotted line represents the upper limit band (20 knots) and blue dotted line indicates the lower limit band (15 knots). In Fig. 2c, EIN15 in situ zonal wind speed is showing large variations in the actual onset date during some of the years. More than 36% in situ zonal wind dataset is not satisfying the IMD onset zonal wind speed criteria. Therefore, over a specified region, a large variation is being observed in EIN15 dataset from its normal wind speed (Srivastava et al. 2013) on the actual onset date. The simulations using CMO ERSST and OI_WK (Fig. 2c, d) are kept within the limit band during the analysis, which causes a mean deviation of ± 5 day from the actual onset for a 30-year time period (from Table 2).

A relation between OLR and zonal wind speed is depicted in Fig. 2, which represents a negative correlation between wind speed and radiation (Bett and Thornton 2016) where the OLR value (Fig. 2a) is reduced with the increase in zonal wind speed (Fig. 2c). This feature is also well simulated in the CMO ERSST as well as CMO OI_WK simulation. The depth of westerly of in situ, CMO ERSST, and CMO OI_WK are maintained at 600 hPa over 0°N–10°N and 55°E–80°E region during the last few days of actual onset (figures not shown). Using the said criteria and by considering the above analysis, we have tried to simulate the onset date for Indian region for a 30-year time period (Table 2), which shows a mean deviation of ± 5 day and a maximum of ± 12 day deviation in CMOs (ERSST and OI_WK) from the actual date of onset. With a robust skill in capturing the intraseasonal monsoon variability, the RegCM has the limitation to simulate the dates in correspondence to in situ observations (Maharana and Dimri 2014, 2016). With the MM5 dynamical core, the RegCM-4.3 has performed moderately in simulation of onset dates and it might be due to the large variation in ICBC over the particular region. Therefore, in this study, we particularly have focused on the physical processes of the data distribution instead to find out the physics behind the uncertainty of the RegCM-4.3 model output.

3.1.2 Active/break phase

To evaluate the model performance in intraseasonal time scale and to analyze the RegCM-4.3 sensitivity with EIN15 downscaled model output with two types of SST, this study has been carried out for another two major phases (active and break) of summer monsoon (Krishnamurti 1985; Krishnamurti and Ardunay 1980). The core region is considered between 71°E–83°E and 21°N–28°N which is closer to the monsoon region of Rajeevan et al. (2010). Active and break periods are considered from the NCC Research Report (2013) as given in (Table 3), which has been identified by standardized rainfall anomaly of greater than + 1 and less than − 1 for minimum three consecutive days respectively. The above criteria were obtained by averaging the daily rainfall over the core monsoon region and by standardizing the daily rainfall data by subtracting from its long-term normal and dividing by its daily SD (Rajeevan et al. 2010). A total of 59 active spells, 44 break spells along with 237 active days, and 246 break days are considered for 30 years during the period 1981–2010 (Table 3). The simulation of intraseasonal monsoon variability during active phases is considered in Figs. 3 and 4. MSLP has an important role for active and break phases (Krishnamurti and Bhalme 1976) and hence considered for further study. The composite analysis of active days for synoptic patterns is spatially distributed in Fig. 3a–i, in which wind circulation at 850 hPa is superimposed on rainfall (Fig. 3a–c), OLR (Fig. 3d–f), and MSLP (Fig. 3 g–i) distributions. Strong monsoon rainfall distribution (Fig. 3a–c) along with the low-level jet (LLJ) over the core region during the active phase is depicted with the CMO ERSST (Fig. 3b) and CMO OI_WK (Fig. 3c), which are closely following the IMD spatial rainfall distribution (Fig. 3a) and temporal pattern (Fig. 4a) during the phases.

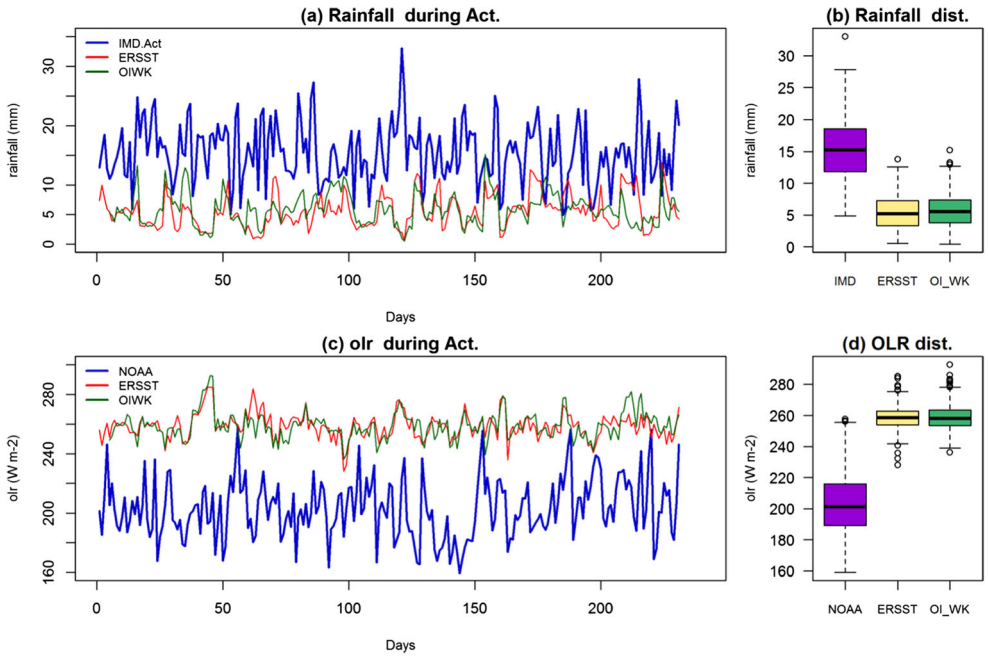

Fig. 4 **a–d** Distribution of rainfall and OLR during active spells of 1981–2010

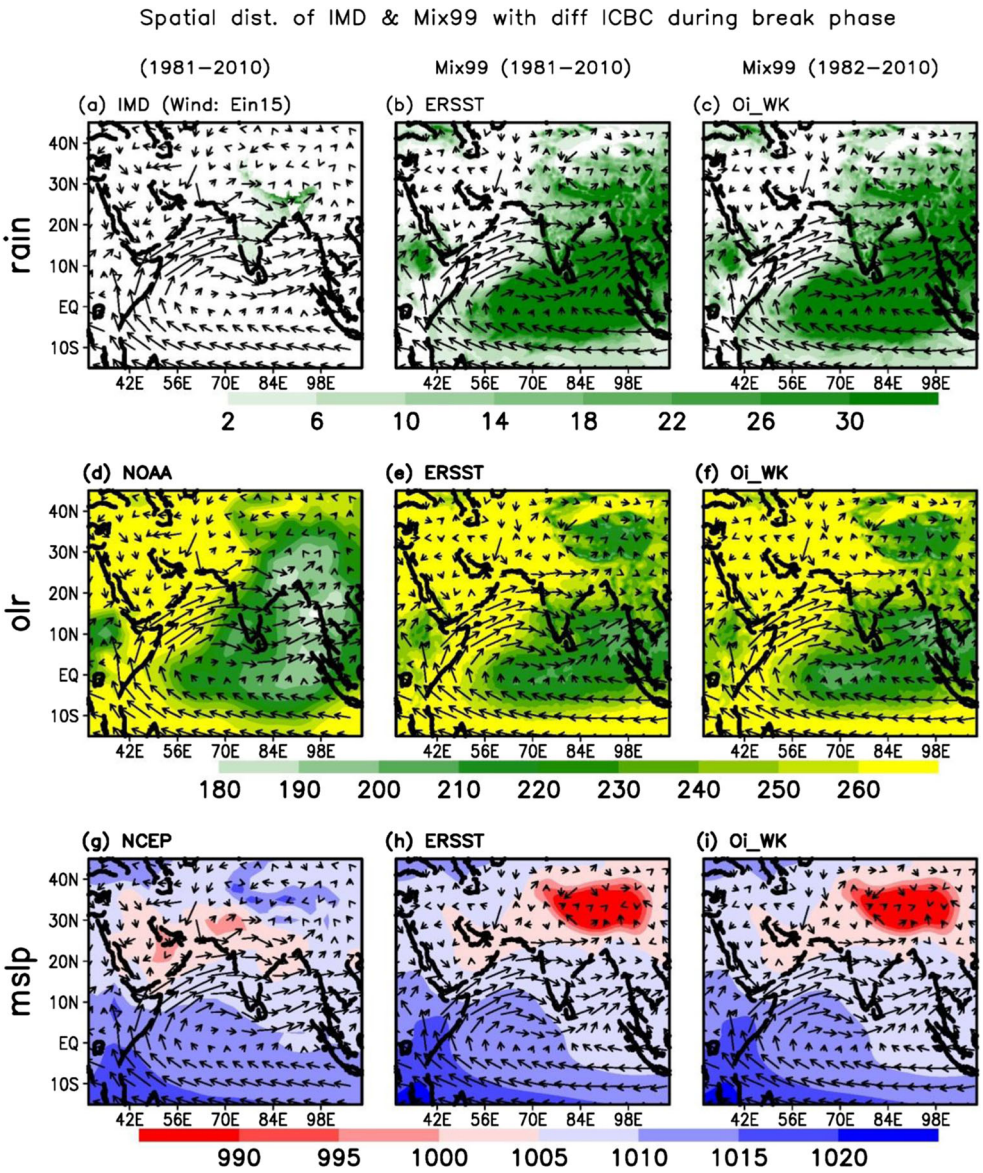

Fig. 5 **a–i** Composite spatial pattern of in situ and CMO-simulated rainfall, OLR, and MSLP distribution during break phases for duration 1981–2010. EIN15 and CMO-derived wind circulation is superimposed at 850 hPa for respective cases

Temporal pattern of CMO rainfall distribution (Fig. 4a–b) is showing a dry bias during this phase. The IMD rainfall (Fig. 4a; blue line) and its distribution (Fig. 4b) are spreaded between 12 to 19 mm of the rainfall amount where CMO ERSST (Fig. 4a; red line) and OI_WK (Fig. 4a; green line) are showing under estimation with 4 to 7 mm (Fig. 4b) of rainfall during the active days. During summer monsoon period, convection plays an important role in forming the cloud, which is inversely correlated with the OLR. Positive/negative anomalies in OLR distribution are the causes of negative/positive rainfall anomaly (Raju et al. 2009). The shrinking/rising distribution of in situ OLR (Fig. 3d) over core region is showing less than 200 Wm^{-2} during the active phase, which is poorly simulated by CMO ERSST (Fig. 3e) and CMO OI_WK (Fig. 3f) OLR distribution. The temporal pattern of CMO OLR (Fig. 4c) is showing warm bias, and its distributions (Fig. 4d) are varying up to 260 Wm^{-2}, whereas NOAA represents 200 Wm^{-2} over the region. ISMR and OLR relationship has been already established in previous study by Raju et al. (2009) and indicated an opposite relationship between ISMR and OLR. In the current study, the CMO OLR distribution are showing warm biases and at the same time, the model-simulated rainfall distribution is representing dry biases. Simultaneously, a pressure belt (Fig. 3) is showing an average pressure of 995–1005 hPa over the Monsoon Convergence Zone (MCZ), and the monsoon trough covers the Gangetic region as a proxy of rainfall distribution and spreads up to foot of the Bay of Bengal (BoB) through the Gangetic plain. Similar results are also provided in the IMD Monsoon Report 2013, which is in agreement with the model-simulated MSLP (Fig. 3 h–

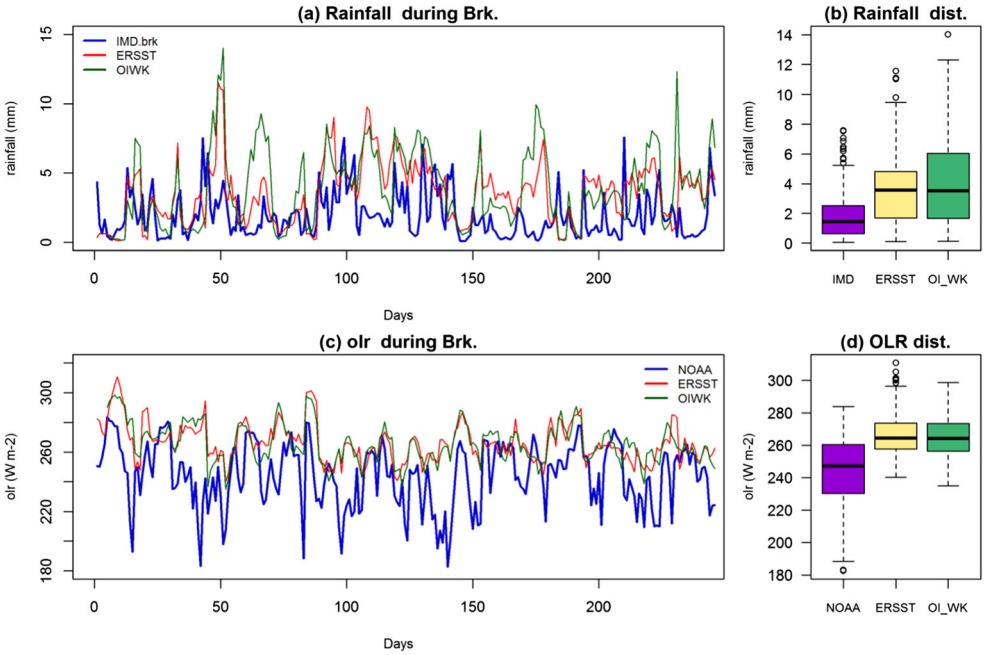

Fig. 6 **a–d** Distribution of rainfall and OLR during break spells of 1981–2010

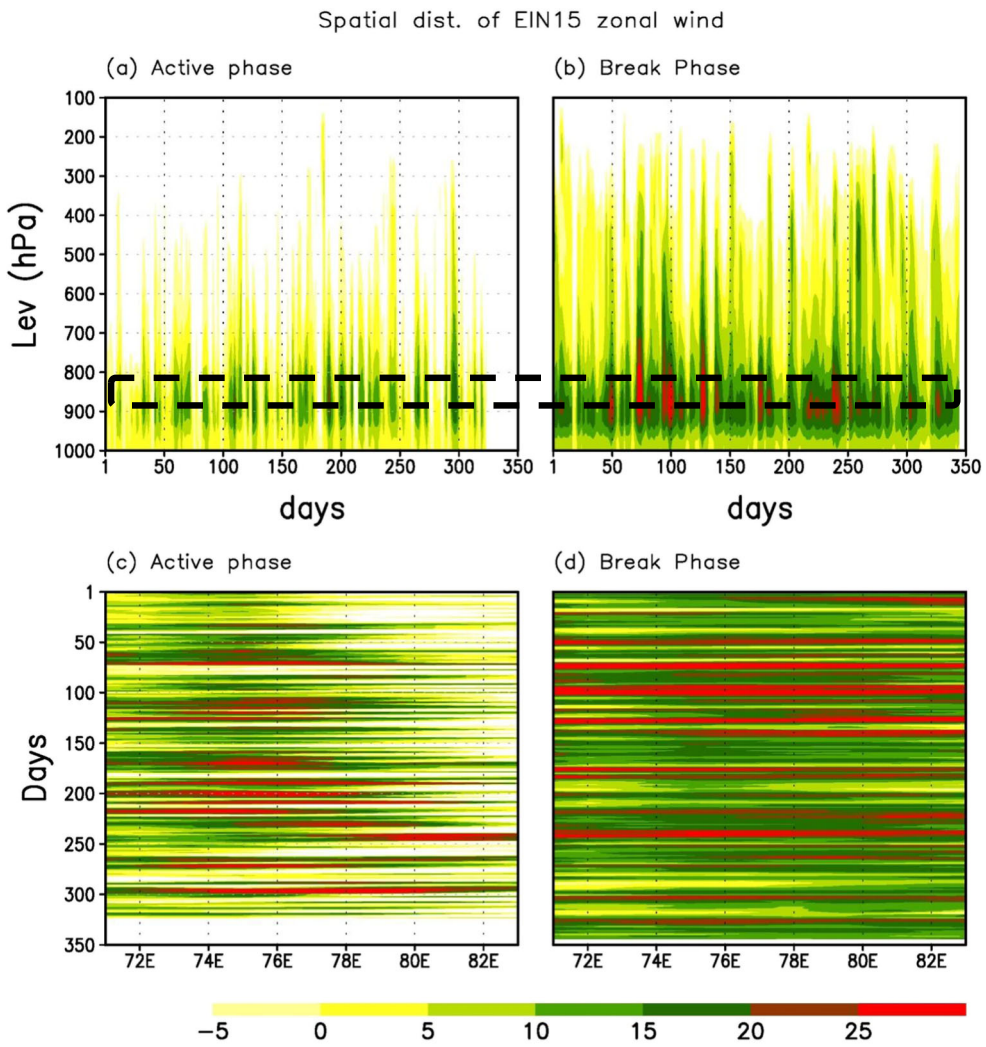

Fig. 7 **a–d** Vertical level-days (**a**, **b**) and days-longitude at 850 hPa (**c**, **d**) of EIN15 zonal wind distribution (Knots/s; shaded) during active and break phase over the core region (71°E-83°E and 21°N-28°N)

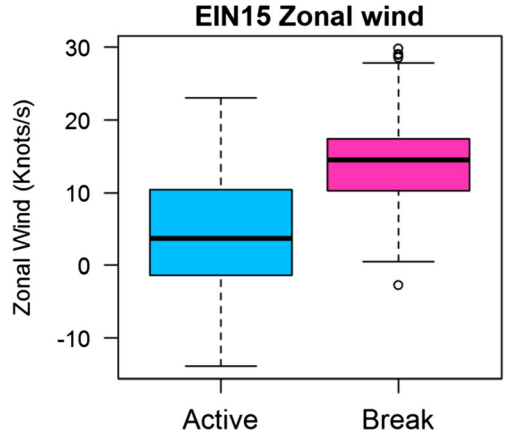

Fig. 8 Distribution of EIN15 zonal wind during active and break phases of Intraseasonal summer monsoon period

i) as compared to NCEP (Fig. 3 g). In in situ MSLP distribution (Fig. 3 g), a low pressure belt of 995–1000 hPa is formed over the MCR and this gradient is not well simulated by the CMOs (Fig. 3 h–i). Due to topographical terrain over the Himalayan region, a deep low-pressure (< 990 hPa) belt is formed in the CMO MSLP (Fig. 3 h–i) and the model is failed to simulate the MSLP over the respective zone. As a proxy parameter in the RegCM rainfall simulation, MSLP does not have a big role in CMO over the MCR. Therefore, non-simulating OLR distribution could be a possible cause behind the agitated rainfall simulation during the active phase.

Composite distribution of synoptic parameters during break phases is spatially distributed in Fig. 5a–i. These figures illustrate a weak monsoon rainfall over the core region, which is depicted well in IMD rainfall distribution (Fig. 5a). CMO ERSST and OI_WK are able to simulate this distribution over the core region (Fig. 5b, c). The temporal rainfall distributions during break phase are considered in Fig. 6a, which indicates that the CMOs are following the rainfall distribution pattern as IMD. Although, the rainfall deviation from the mean is slide high for CMO ERSST and OI_WK rainfall as compared to IMD rainfall (Fig. 6b). The less OLR distributed area is shifted towards the eastern part from the core region of India (Fig. 5d–f) and found more than 220 Wm^{-2} over the Indian core region during this phase (Raju et al. 2009). Temporal distributions of the CMO analyses are also capturing the peak as NOAA OLR (Fig. 6c) with a slight over estimation in respect to in situ (Fig. 6d). At the same time, the monsoon trough in Fig. 5 g–i has been shifted towards the Himalayan foothills from the Gangetic plain and has extinct from BoB foot (Bhatla and Ghosh 2015). During the break phase, the pressure belt (995–1005 hPa) generally remains active and spreads over the Gangetic plain during the active period and shifted to the Himalayan foothill in in situ (Fig. 5 g) as well as CMOs (Fig. 5 h–i) and monsoon, while become weaker over the core region. These are the prominent feature during the break phases of ISMR and well simulated by different CMOs of Mix99 CPSs. The spatial gradient is also well simulated by CMOs over all the remaining part including BoB, Arabian Sea, and Indian Ocean (except the Himalayan foothill region) during active/break phases. Another major dependency of model performance is the ICBC. Therefore, to find out the possible causes behind disturbed rainfall and non-simulating the OLR distribution, the role of the RegCM's ICBC for long-term simulation is carried out in further section.

3.2 Dependencies of RegCM-4.3 output on lateral boundary conditions

The above study shows that the sensitivity of model-simulated rainfall, OLR, MSLP, and zonal wind distributions over Indian subcontinent is showing an over or under estimation in simulating different phases of ISMR. Lateral boundary conditions of u and v wind components, surface pressure, temperature, and water vapor along with SSTs specified over the ocean are the regulators and are used to run the RegCM-4.3 over the specified region. The study of Bett and Thornton (2016) has shown the relationship of these parameters and responses to rainfall simulation. Zonal wind disturbances have been identified as the main mechanism in organizing rainfall pattern over a particular region (Diedhiou et al. 1999). Therefore, to find out possible causes behind the uncertain behavior of

Table 4 Statistical scores of the RegCM-4.3 simulation with in situ during the phases of monsoon

	Onset phase				Active phase				Break phase			
	OLR		U-wind		Rainfall		OLR		Rainfall		OLR	
	SD	BIAS	SD	BIAS	SD	BIAS	SD	BIAS	SD	BIAS	SD	BIAS
In situ	29.24		4.46		5.06		20.02		1.65		21.50	
ERSST	12.26	− 2.77	1.32	− 1.54	2.84	− 9.8	8.56	55.68	2.25	− 1.60	13.16	− 22.28
OI_WK	11.68	− 3.2	1.87	− 1.08	2.71	− 9.5	9.22	55.82	2.76	− 2.04	13.18	− 21.8

Mix99 CPS, we focused on the ICBC (specially zonal wind) provided for model run. Figure 7a–d represents Hovmöller diagram of vertical level wind structure-days (Fig. 7a–b) and days-longitude-wise distribution (Fig. 7c–d) of EIN15 zonal wind at 850 hPa during active and break phases over the Indian core region. The shaded area

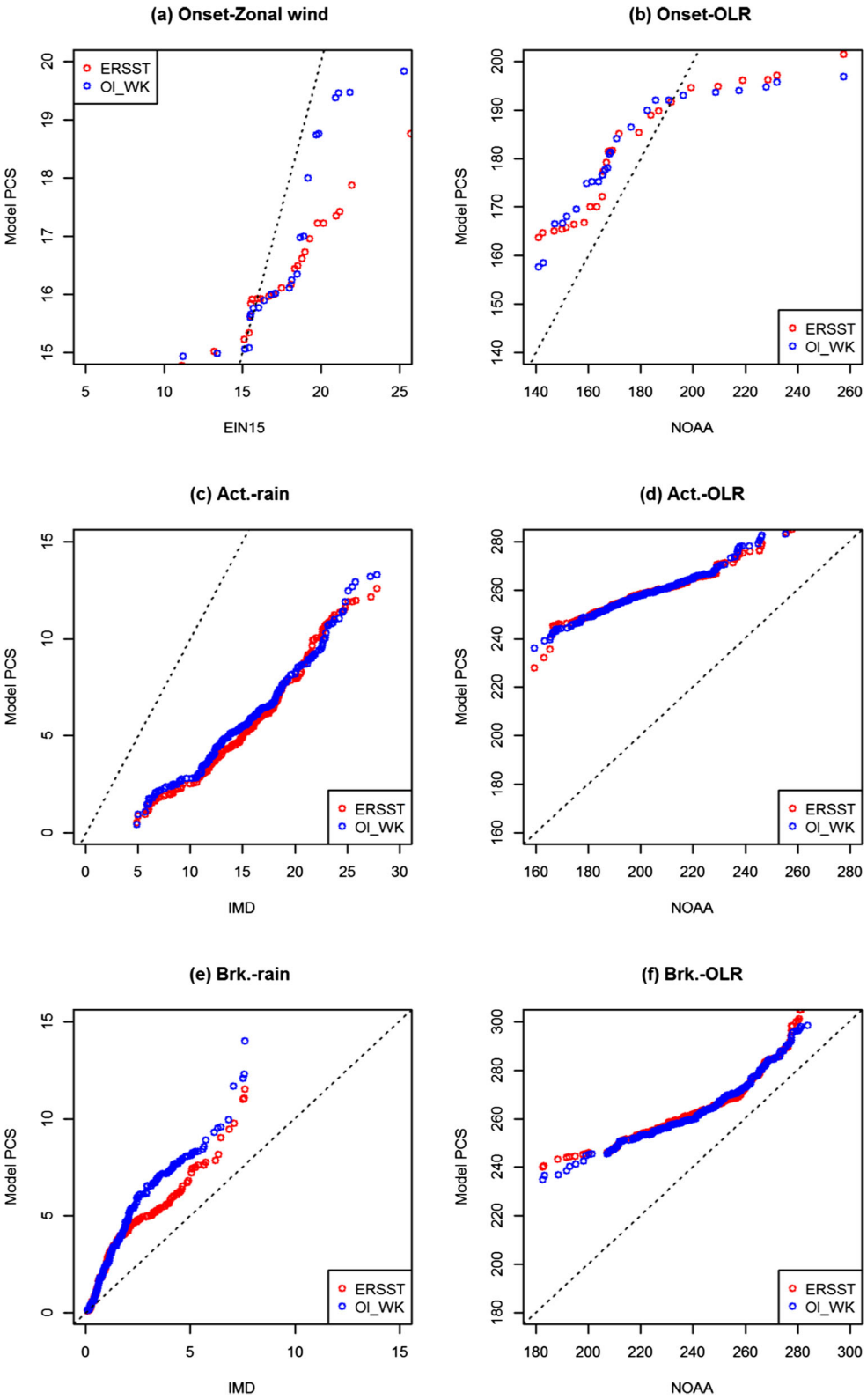

Fig. 9 **a–f** Q-Q distribution of different synoptic parameters during onset, active, and break phase in respect to in situ dataset with 5% significant level

represents the zonal wind speed in knots/s. This distribution illustrates the low efficiency of zonal wind distribution with the color shaded of 0–15 knots/s during active phase (Fig. 7a) and 10–20 knots/s on vertical level 900–800 hPa during break phase (Fig. 7b). Generally, LLJ usually blows over the Indian subcontinent with a higher speed during the active condition than the weak and normal monsoon conditions (Ruchith et al. 2014). But EIN15 zonal speed circulation speed never achieved a value over 25 knots/s at the lower level. At 850 hPa, most of the active days attained wind speed of 0–10 knots/s and very few cases are there that achieved more than 15 knots/s during the active days (Fig. 7c). During the break conditions, the wind speed has shown an average of 10–25 knots/s (Fig. 7d) over the region. The study by Ruchith et al. (2014) and Varikoden (2006) showed that during active phase, the zonal wind blows with a higher speed over the core region rather than the normal and weak monsoon condition. Zonal wind blows from the Arabian Sea with the core speed of ~ 34 knots/s and crosses through the central India (core region) with average speed of ~ 28 knots/s at 850 hPa during active phase. During break phase, the direction of LLJ turns towards south and becomes weak and blows with a speed of less than ~ 15 knots/s (Varikoden 2006). In Fig. 8, box plot has been considered for clear representation of in situ zonal wind distribution which represents the EIN15 zonal wind distribution during active and break days with 25 and 75 percentile over the region. With a mean of 4 knots/s, in situ EIN15 zonal wind is blowing over the core region during active phase and in break phase, the mean speed is elevated up to 14 knots/s. Therefore, a sharp conclusion of the above figure might be drawn that the in situ zonal wind speed is showing a large under estimation in speed during active phase, whereas a higher speed is expected during the active phase. The dynamics of zonal wind circulation pattern during active and break phases of summer monsoon showed a large bias (~ 24 knots/s) in in situ zonal wind speed at 850 hPa during the active phase. During the break phase, the EIN15 zonal wind speed follows its regular condition (speed of less than ~ 15 knots/s) and blows with the speed ~ 14 knots/s.

Rainfall is the most chaotic factor depends upon a combination of five environmental factors, and zonal wind is one of them. The model-simulated rainfall distribution purely depends on the ICBC in situ components. Therefore, a large bias in in situ distribution will have a direct impact in the model-simulated rainfall distribution. In this study, the lack/excess of zonal wind circulation speed during the ISM season is carried forward during model simulation process. Due to the negative correlation between the zonal wind speed and OLR distribution, the in situ zonal wind distribution forces the CMO OLR simulation. At the same time, the disturbance in OLR distribution affects the excess/lack of rainfall distribution over the rain belt area (Diedhiou et al. 1999) in the RegCM-4.3 simulation during the intraseasonal monsoon season (Sylla et al. 2010, 2011).

3.3 Statistical score and model verification

3.3.1 Statistical scores and biases

Table 4 represents the statistical scores of model-simulated output and in situ data during different phases of monsoon. Statistical representation of CMOs have showed less than half of SD in ERSST, OI_WK CMO OLR, and U-wind distribution with respect to the in situ during onset phase and the bias over the respective region, which represents dry for the parameters of OLR and zonal wind. Previous analyses (Section 4.1) showed a high fluctuation in in situ over the respective region, and the mean for a 30-year period has induced the analyses to disfavor the CMO performance. In this study, onset simulations by CMOs are considered following the IMD criteria; therefore, the biases are unexpected in model simulation, which lay the overestimation in in situ datasets. During active/break phases, the SD in CMO rainfall and OLR is depicted roughly a half of in situ, while biases represent the opposite relationship among rainfall and OLR distribution with high positive biases in OLR as stated in the above section. The bias in OLR distribution over the core region is higher during active period than break period, which attains about double in respect to break phase. Analyses from Section 4.1 and Section 4.2 showed the mechanism of ICBC in the RegCM and impact of wind circulation on OLR as well as rainfall distribution, and a relationship between zonal wind, OLR, and rainfall is also evident in the observed datasets. Those sections particularly dealing with the uncertainties in the RegCM rainfall simulation due to disturbed ICBC over some specified region during different phases of ISM, where this section supporting the analyses and highlighting the nature of CMOs by the statistical score rather than verifying the model with the in situ itself.

3.3.2 Model verification

Verification statistics of CMOs are considered using Q-Q distribution and ECDF for the considered parameters for the synoptic analysis during the phases of ISMR.

Q-Q plot is a probability plot to compare the shapes of distribution between two data series (Wilk and Gnanadesikan 1968) or for its theoretical distribution itself

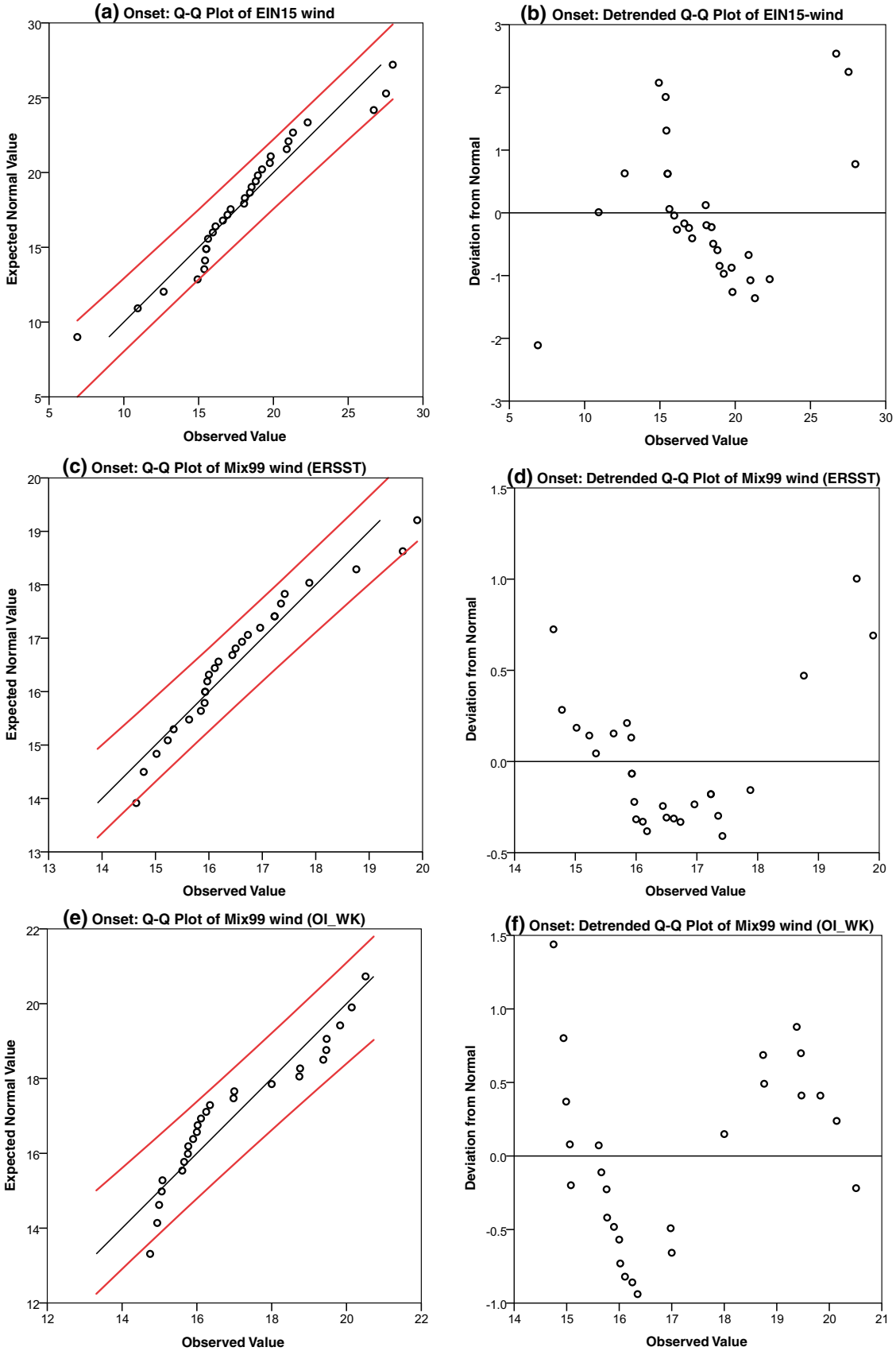

Fig. 10 **a–l** Q-Q distribution of the individual datasets with 1% significant band along with the detrended Q-Q distribution of the respective dataset considered for onset simulation

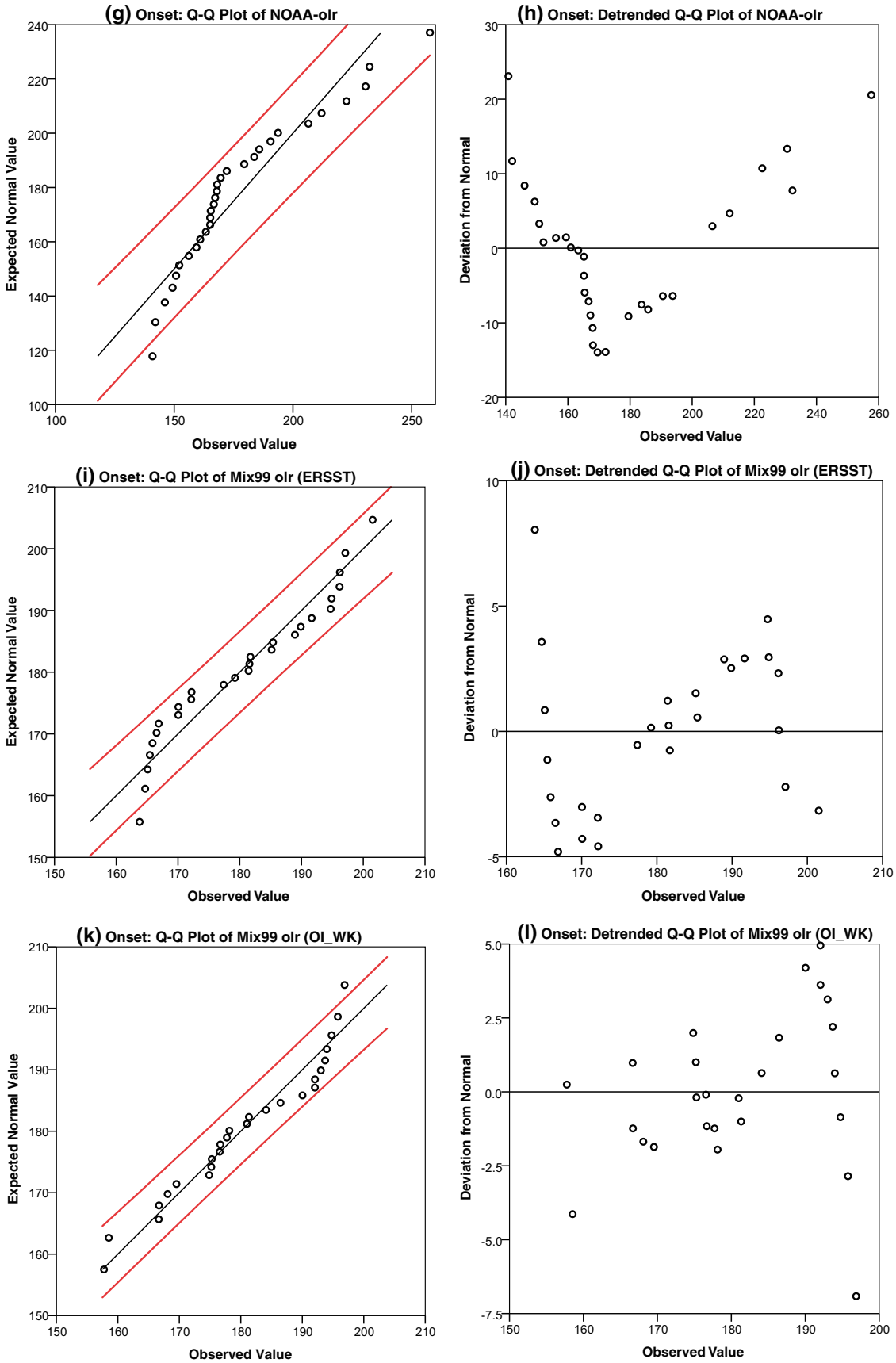

Fig. 10 (continued)

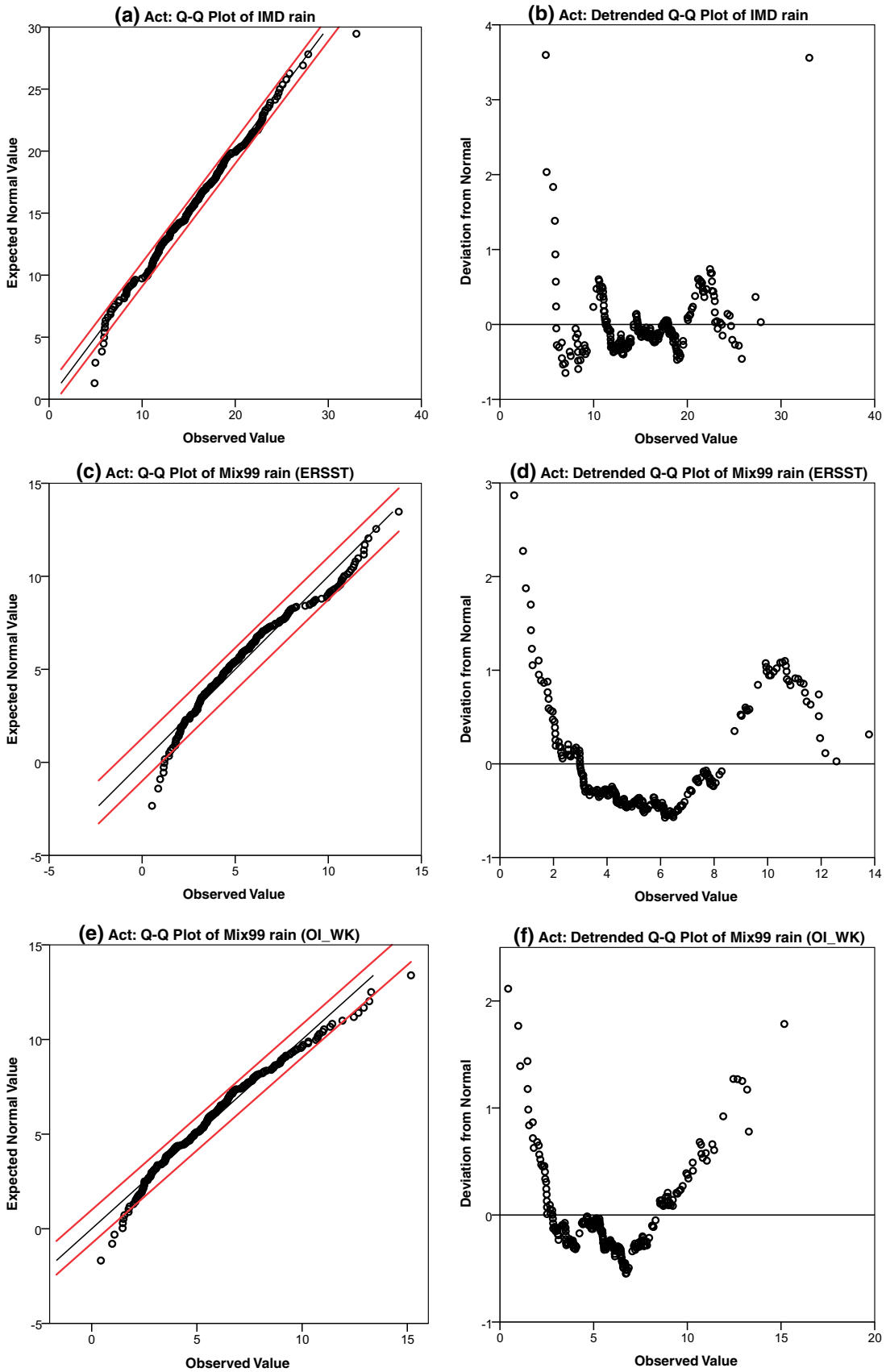

Fig. 11 **a–l** Q-Q distribution of the individual datasets with 1% significant band along with the detrended Q-Q distribution of the respective dataset considered for active phase simulation

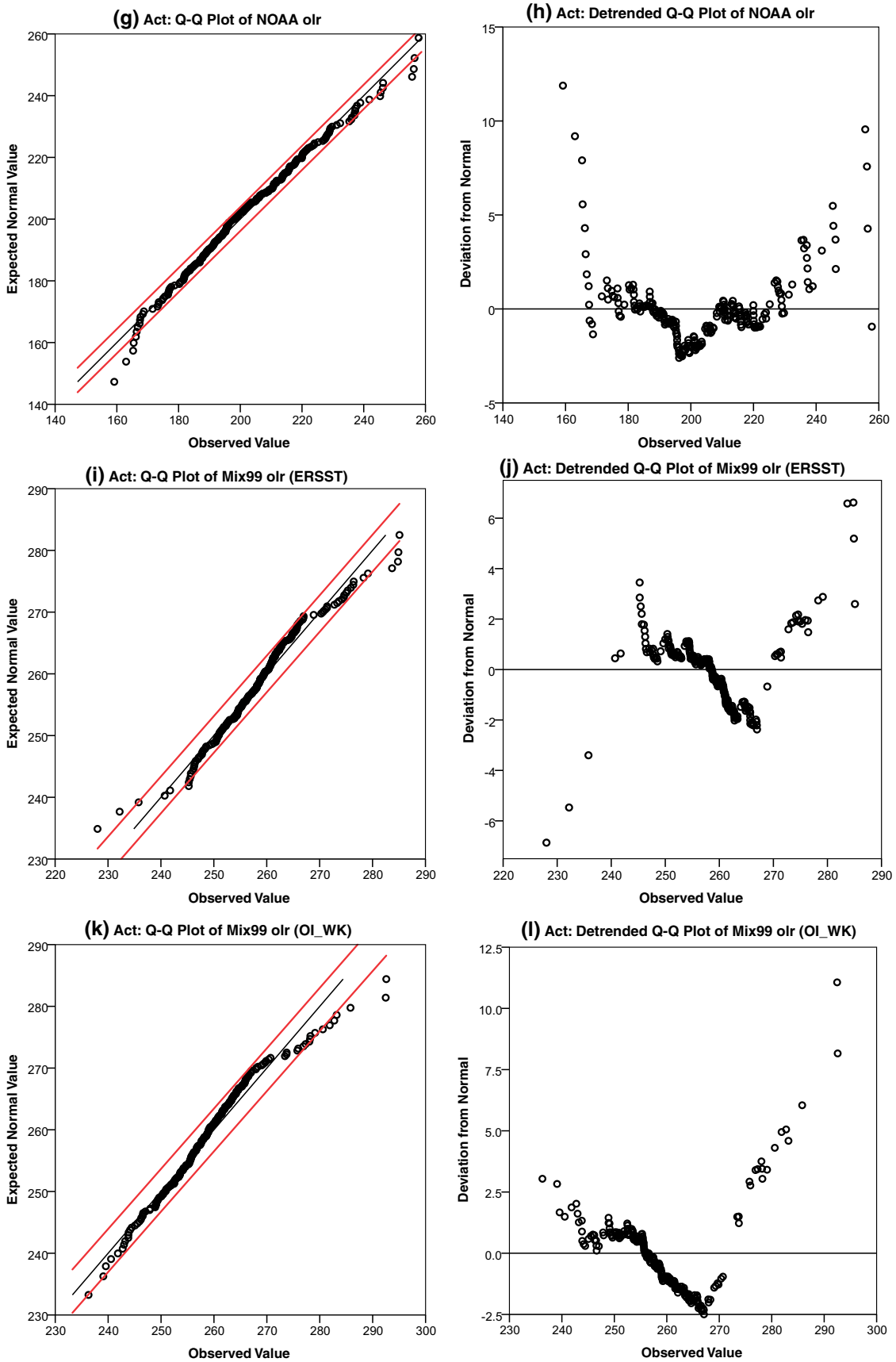

Fig. 11 (continued)

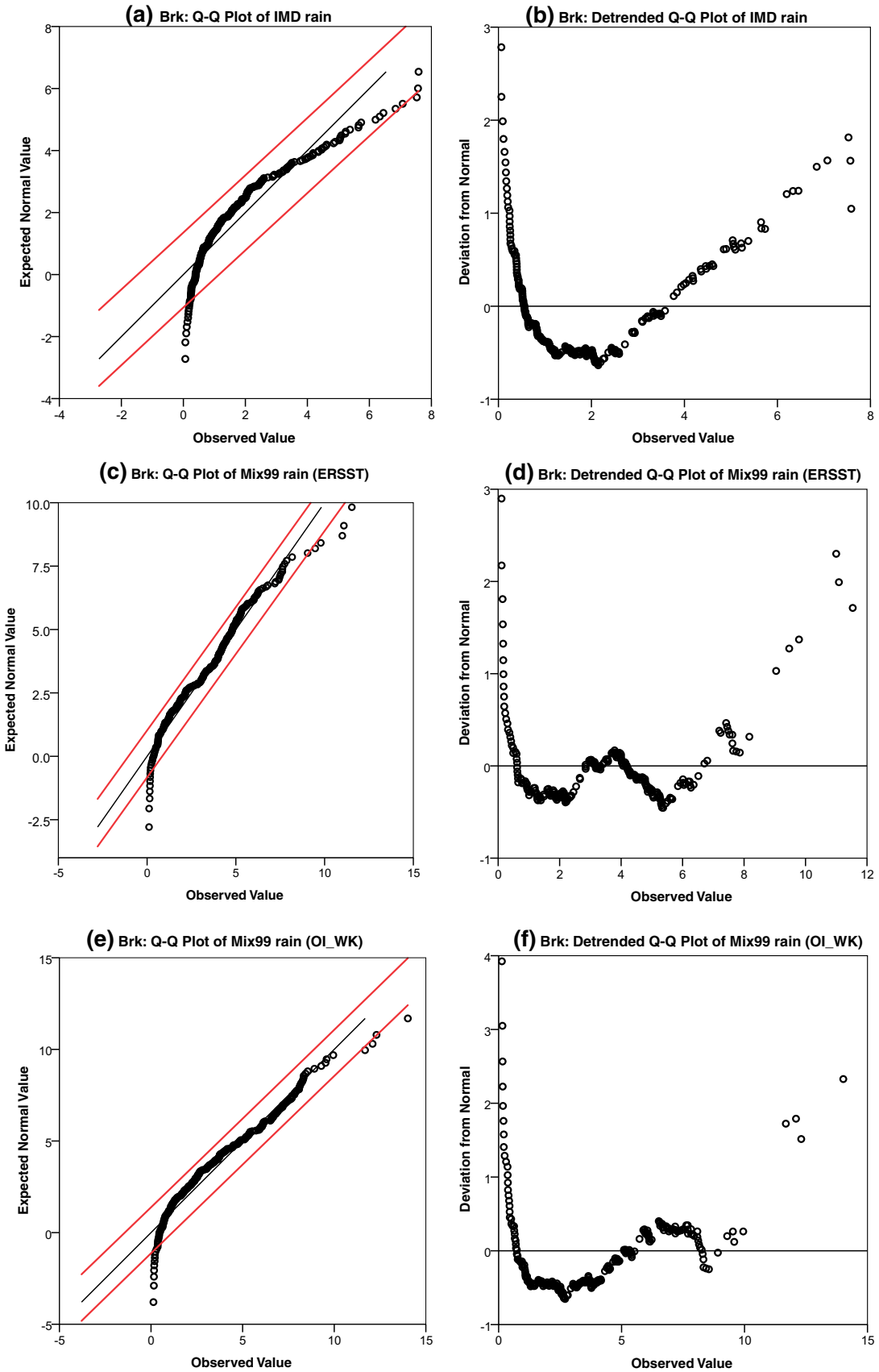

Fig. 12 **a–l** Q-Q distribution of the individual datasets with 1% significant band along with the detrended Q-Q distribution of the respective dataset considered for break phase simulation

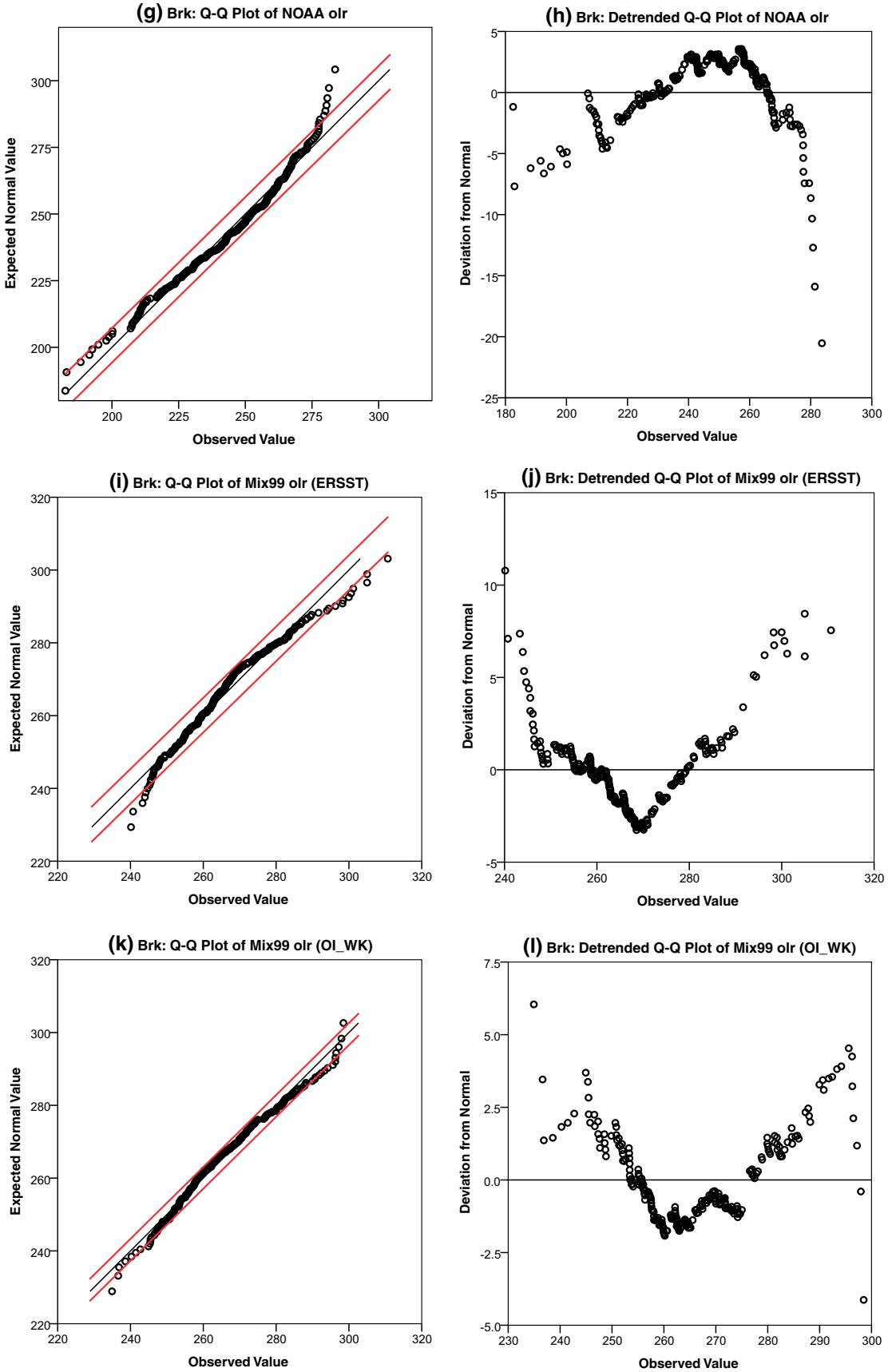

Fig. 12 (continued)

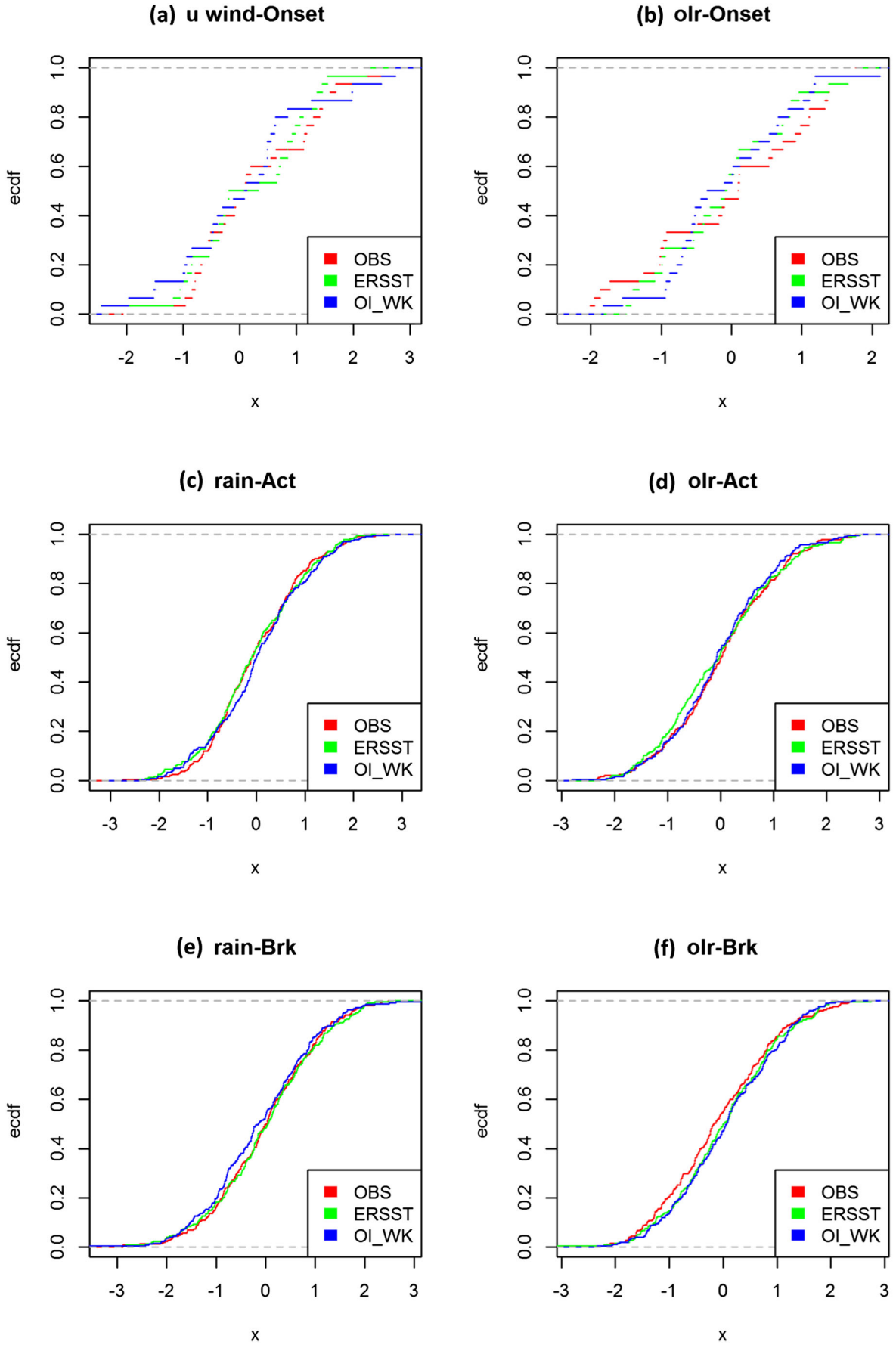
(a) u wind-Onset
(b) olr-Onset
(c) rain-Act
(d) olr-Act
(e) rain-Brk
(f) olr-Brk
ecdf
x
OBS
ERSST
OI_WK

◀ **Fig. 13** **a–f** Empirical cumulative distribution function (ECDF) of different parameter during onset, active and break phase of ISM

(Singh et al. 2014). This distribution verifies the probability by plotting quantile graphic against each other or with its theoretical distributions to understand the properties of data. The graphical representation of Q-Q plot (Fig. 9a–f) generally used to compare the CMO performance with a nonparametric approach along with their distributions with respect to in situ datasets at 5% level of significance. The scatters in x- and y-axes correspond to one of the quantile of second distribution (y-coordinate) and plotted against same quantile of first distribution (x-coordinate). If CMOs and in situ data distributions have similarity, then the quantiles will be laid approximately on the dashed line with 45° angle. Otherwise, if distributions are linearly related, then the scatters will be laid approximately on a line. But it is not necessarily to be laid on the line $y = x$. The red scatters indicate the distribution of ERSST CMO, while blue is for OI_WK CMO. For checking the goodness of fit of CMOs with in situ quantiles, most of the datasets during onset are near to linear line. A slight under estimation is depicted in CMO's zonal wind speed during onset phase with respect to in situ quantiles (Fig. 9a). At the same time, an overestimation is also observed in OLR distribution among the CMOs and in situ quantiles (Fig. 9b). The wind and OLR distributions are showing a clear opposite relationship during the ISM onset. Figure 9c–f represents their goodness of fit with in situ by showing their sequentially congested distribution of data. Although, during active phase, the model-simulated output suffers from lack of rainfall distribution in comparison to the in situ and their quantiles are showing under estimation with in situ observation (Fig. 9c). On other side, due to surplus in OLR distribution with in situ, the quantiles (Fig. 9d) are showing an overestimation during active phase. During break phases, the scatters (Fig. 9e–f) are very close to in situ and the quantiles for rainfall distribution are showing goodness for CMO (Fig. 9e). The model-simulated OLR quantiles of different CMOs are found very close to the linear line (Fig. 9f). It is also observed that the ERSST CMO is showing better performance with in situ than the CMO OI_WK. On the other hand, the CMO ERSST is showing its quantiles a bit nearer to the in situ or it is overlapping over CMO OI_WK.

For further verification of CMOs and in situ datasets with their respective normal quantiles, Figs. 10 and 12 have been considered for the respective parameters during the phases of monsoon. In these figures, the normal Q-Q plots represent the validation of the data with the distributional assumption of the respective dataset by providing visual comparison of the sample quantiles to the corresponding theoretical quantiles. Detrended normal Q-Q plots have also been considered for monitoring the deviation of the actual data from its normal. All the figures represent their significance with 1% significant band. The normal Q-Q plot for all the parameters of in situ as well as CMOs are plotted in Fig. 10 for onset, Fig. 11 for active phase, and Fig. 12 for break phase simulation. These figures are showing the goodness of fit with their theoretical distributions itself by illustrating their fitness over the linear line with 1% significant band (Fig. 10a, c, e, g, i, and k). The detrended normal Q-Q plots show a goodness of fit for every monsoon phase by representing the crowds of scatters from the normal. It has been also observed that the deviation of CMO data from its normal is much less than in situ (Fig. 10b: IMD rain, Fig. 10h: NOAA OLR) distribution either in the case of rainfall (Fig. 10d, f) or OLR (Fig. 10j, l). With a slight deviation from the normal, the quantiles are gathered together over the line during active and break phases and their detrended normal are also showing a high significance with less deviation (Fig. 11a–l and Fig. 12a–l). ECDF (Fig. 13a–f) is another nonparametric statistical estimator tools to interpret similar groups of random datasets by their own distributions (Gibbons and Chakraborti 2003, 1992). In this ECDF estimator, it is possible to visualize the data series distribution by the slope of the line and with the increase of ECDF from 0 to 1. Because of the limited number of data series, the curve in Fig. 13a, b looks rough rather than smooth. The ECDF fitted results of three distributions (in situ, ERSST, and OI_WK) for every single parameter is presented in one box. These boxes of different parameters and different phases showed that the CMO ERSST and CMO OI_WK are very close to the in situ distribution and following the pattern of in situ for every ECDF key quantile. The overall statistical study shows a clear distribution pattern for all the synoptic parameters in CMO ERSST and OI_WK considered for the analysis of onset, active, and break phase with respect to the in situ. Their distribution patterns are showing goodness of fit with in situ observation and their theoretical distributions itself. This section deals with the validation of the RegCM output with in situ during different phases with statistical inference which performs well in comparison to in situ. In other words, the RegCM follows the ICBC with some over/under estimation in the model simulation.

4 Summary and conclusions

The study indicates the sensitivity of the RegCM simulation for ISM with different lateral boundary conditions. In order to evaluate the causative factors behind the uncertainties in the

RegCM simulation, various factors are considered and subsequently analyzed. The conclusions of this study are as follows:

Sensitivity of RegCM's Mix99 (Grell->Land & Emanuel->Ocean) CPS has a minor dependency with the ERSST and OI_WK SST lateral boundary conditions in simulating the intraseasonal variability of ISM.

The zonal wind of EIN15 reanalysis ICBC lacks enough speed over the core Indian region and around Kerala during definite rainy days (onset and active phases) of ISMR.

Model-simulated rainfall distribution entirely depends on the distribution of in situ ICBC and the disturbed zonal wind distribution in EIN15, which is being carried forward in the RegCM simulation process.

Statistical distribution of all the parameters are in agreement with their respective theoretical quantiles and in situ distribution, and CMOs are following the pattern of in situ datasets with some under/over estimation, which illustrates the RegCM capabilities towards ISM simulation.

The RegCM is able to capture the prominent data distribution very well during the phases of monsoon, if an unbiased ICBC is provided.

Therefore, it is advised to cross verify the ICBC over the specified study region before using it directly for the RegCM simulations.

Acknowledgements This work is a part of a R&D project, funded by the Department of Science and Technology (DST), Ministry of Earth Science (MoES), Govt. of India. The authors wish to thank to The India Meteorology Department (IMD), NOAA/OAR/ESRL (Boulder, Colorado, USA; http://www.esrl.noaa.gov/psd/), and European Centre for Medium-Range Weather Forecasts (ECMWF) for providing gridded datasets. The authors seem their sincere gratitude to Prof. T.N. Krishnamurti, Florida State University, USA for his valuable comments on the manuscript to improve publication quality. Special thanks to the International Center for Theoretical Physics (ICTP), Italy, for providing the RegCM. The authors wish to extend their sincere gratitude to the Journal Editor and the Reviewers for their insightful comments on the paper.

References

Almazroui M (2016) RegCM4 in climate simulation over CORDEX-MENA/Arab domain: selection of suitable domain, convection and land-surface schemes. Int J Climatol 36:236–251

Almazroui M (2012) Dynamical downscaling of rainfall and temperature over the Arabian Peninsula using RegCM4. Clim Res 52:49–62

Arakawa A, Schubert WH (1974) Interaction of a Cumulus Cloud Ensemble with the Large-Scale Environment, Part I. J. Atmos. Sci. 31: 674-701. https://doi.org/10.1175/1520-0469(1974)031<0674:IOACCE>2.0.CO;2

Bett PE, Thornton HE (2016) The climatological relationships between wind and solar energy supply in Britain. Renew Energy 87:96–110

Bhatla R, Ghosh S, Mandal B, Mall RK, Sharma K (2016) Simulation of Indian summer monsoon onset with different parameterization convection schemes of RegCM-4.3. Atmos Res 176–177:10–18. https://doi.org/10.1016/j.atmosres.2016.02.010

Bhatla R, Ghosh S (2015) Study of break phase of Indian summer monsoon using different parameterization schemes of RegCM4.3. Int. J. Eart. Atmos Sci 2(3):109–115

Central Statistical Organization (1998) Compendium of environment statistics. Central Statistical Organization, Department of Statistics, Ministry of Planning and Program Implementation, Government of India: New Delhi

Collins WD, Bitz CM, Blackmon ML, Bonan GB, Bretherton CS, Carton JA, Chang P, Doney SC, Hack JJ, Henderson TB, Kiehl JT, Large WG, McKenna DS, Santer BD, Smith RD (2006) The community climate system model version 3 (CCSM3). J Clim 19:2122–2143

Dash SK, Pattnayak KC, Panda SK, Vaddi D, Mamgain A (2015) Impact of domain size on the simulation of Indian summer monsoon in RegCM4 using mixed convection scheme and driven by HadGEM2. Clim Dyn 44:961–975

Dash SK, Shekhar MS, Singh GP (2006) Simulation of Indian summer monsoon circulation and rainfall using RegCM3. Theor Appl Climatol 86:161–172

Dickinson RE, Errico RM, Giorgi F, Bates GT (1989) A regional climate model for the Western United States. Clim Chang 15:383–422

Diedhiou A, Janicot S, Viltard A, de Felice P, Laurent H (1999) Easterly wave regimes and associated convection over West Africa and tropical Atlantic: results from NCEP/NCAR and ECMWF reanalyses. Clim Dynam 15:795–822

Dobler A, Ahrens B (2010) Analysis of the Indian summer monsoon system in the regional climate model COSMO-CLM. J Geophys Res 115:1–12

Elguindi N, Bi X, Giorgi F, Nagarajan B, Pal J, Solmon F, Giuliani G (2013) Regional climate model RegCM user manual version 4. 4. The Abdus Salam International Centre for Theoretical Physics, StradaCostiera, Trieste, Italy, 54 pp.

Emanuel KA (1991) A scheme for representing cumulus convection in large-scale models. J Atmos Sci 48(21):2313–2335

Emanuel KA, Živković-Rothman M (1999) Development and evaluation of a convection scheme for use in climate models. J Atmos Sci 56: 1766–1782

Fritsch JM, Chappell CF (1980a) Numerical prediction of convectively driven mesoscale pressure systems. Part I: convective parameterization. J Atmos Sci 37:1722–1733

Fritsch JM, Chappell CF (1980b) Numerical prediction of convectively driven mesoscale pressure systems. Part II: mesoscalemodel. J Atmos Sci 37:1734–1762

Gibbons JD, Chakraborti S (1992) Nonparametric statistical inference. 3rd edition: Marcel Dekker

Gibbons JD, Chakraborti S (2003) Nonparametric statistical inference. Marcel Dekker, New York

Giorgi F, Anyah RO (2012) The road towards RegCM4. Clim Res 52:3–6. https://doi.org/10.3354/cr01089

Giorgi F, B Hewitson, J Christensen, M Hulme, H Von Storch, P Whetton, R Jones, L Mearns, C Fu, (2001). Regional climate information: evaluation and projections (chapter 10). In climate change 2001: the scientific basis, contribution of working 32 group I to the third assessment report of the IPCC [Houghton, J. T. Y. Ding, D. J. Griggs, M. Noguer, P. J. Van der Linden, X. Dai, K. Maskell, and C. A. Johnson (eds.)]. Cambridge U. Press: Cambridge, pp. 739–768

Giorgi F, Bates GT (1989) The climatological skill of a regional model over complex terrain. Mon Weather Rev 117:2325–2347

Giorgi F, Coppola E, Solmon F, Mariotti L, Sylla MB, Bi X, Elguindi N, Diro GT, Nair V, Giuliani G, Turuncoglu UU, Cozzini S, Güttler I, O'Brien TA, Tawfik AB, Shalaby A, Zakey AS, Steiner AL, Stordal F, Sloan LC, Brankovi'c C (2012) RegCM4: model description and preliminary tests over multiple CORDEX domains. Clim. Res 52:7–29. https://doi.org/10.3354/cr01018

Grell GA (1993) Prognostic evaluation of assumptions used by cumulus parameterizations. Mon Wea Rev 121(3):764–787

Grell GA, Dudhia J, Stauffer DR (1994) Description of the fifth-generation Penn State/NCAR Mesoscale Model (MM5). National Center for Atmospheric Research (NCAR) Technical Note NCAR/TN-398+STR, NCAR, Boulder, CO. doi: https://doi.org/10.5065/D60Z716B

Holtslag AAM, de Bruijn EIF, Pan HL (1990) A high resolution air mass transformation model for short-range weather forecasting. MonWeather Rev 118:1561–1575

IMD Monsoon report (2013) Monsoon 2013: a report. (edited by D. S. Pai and S.C. Bhan), India Meteorological Department (IMD), Government of India. IMD Met Monograph: ESSO/IMD/SYNOPTIC MET/01-2014/15

Kiehl JT, Hack JJ, Bonan GB, Boville BA, Breigleb BP, Williamson D, Rasch P (1996) Description of the NCAR community climate model (CCM3). Technical Report NCAR/TN-420+STR, National Center for Atmospheric Research, Boulder, CO. doi: https://doi.org/10.5065/D6FF3Q99

Krishnamurthy V, Kinter III JL (2003) The Indian monsoon and its relation to global climate variability. Global Climate (X. Rodó and F. A. Comín, Eds., Springer-Verlag) 186–236

Krishnamurti TN (1985) Summer monsoon experiment: a review. Mon. Wea. Rev. 113:1590–1626

Krishnamurti TN, Ardunay P (1980) The 10–20 day westward propagating model and 'break' in the monsoon. Tellus 32:15–26

Krishnamurti TN, Bhalme HN (1976) Oscillations of monsoon system. Part I: observational aspects J Atmos Sci 45:1937–1954

Maharana P, Dimri AP (2014) Study of seasonal climatology and interannual variability over India and its sub-regions using a regional climate model (RegCM3). J. Earth. Sys. Sci. 123(5):1147–1169

Maharana P, Dimri AP (2016) Study of intraseasonal variability of Indian summer monsoon using a regional climate model. Clim Dyn 46(3):1043–1064

Maurya RKS, Sinha P, Mohanty MR, Mohanty UC (2017) Coupling of community land model with RegCM4 for Indian summer monsoon simulation. Pure Appl Geophys 174:4251–4270. https://doi.org/10.1007/s00024-017-1641-8

Mishra V, Kumar D, Ganguly AR, Sanjay J, Mujumdar M, Krishnan R, Shah RD (2014) Reliability of regional and global climate models to simulate precipitation extremes over India. J Geophys Res Atmos 119:9301–9323

NCC Research Report (2013) Development and analysis of a new high spatial resolution (0.25o x 0.25o) long period (1901-2010) daily gridded rainfall data set over India. [Ed/author: D. S. Pai, Latha Sridhar, M. Rajeevan, O. P. Sreejith, N.S. Satbhai and B. Mukhopadhyay]. NCC Research Report No 1/2013. 63

Pai DS, Rajeevan M (2007). Indian summer monsoon onset: variability and prediction. National Climate Centre, India Meteorological Department

Park S, Hong SY (2004) The role of surface boundary forcing over South Asia in the Indian summer monsoon circulation: a regional climate model sensitivity study. Geophys Res Lett 31:L12112. https://doi.org/10.1029/2004GL019729

ParthSarthi P, Ghosh S, Kumar P (2015) Possible future projection of Indian summer monsoon rainfall (ISMR) with the evaluation of model performance in coupled model inter-comparison project phase 5 (CMIP5). Glob Planet Chan 129:92–106

ParthSarthi P, Kumar P, Ghosh S (2016) Possible future rainfall over the Gangetic Plains (GP), India, in multi model simulations of CMIP3 and CMIP5. Theor Appl Clim 124(3–4):691–701

Rajeevan M, Gadgil S, Bhate J (2010) Active and break spells of the Indian summer monsoon. J Earth Sys Sci 119(3):229–247

Raju PVS, Bhatla R, Almazroui M, Assiri M (2015) Performance of convection schemes on the simulation of summer monsoon features over the South Asia CORDEX domain using RegCM-4.3. Int J Climatol 35:4695–4706. https://doi.org/10.1002/joc.4317

Raju PVS, Bhatla R, Mohanty UC (2009) The evolution of mean conditions of surface meteorological fields during active/break phases of the Indian summer monsoon. Theor Appl Climatol 95:135–149

Ruchith RDP, Raj E, Kalapureddy MCR, Deshpande SM, Dani KK (2014) Time evolution of monsoon low-level jet observed over an Indian tropical station during the peak monsoon period from high-resolution Doppler wind lidar measurements. J Geophys Res Atmos 119:1786–1795. https://doi.org/10.1002/2013JD020752

Saeed F, Hagemann S, Jacob D (2009) Impact of irrigation on the South Asian summer monsoon. Geophys Res Lett 36:L20711. https://doi.org/10.1029/2009GL040625

Singh D, Tsiang M, Rajaratnam B, Diffenbaugh NS (2014) Observed changes in extreme wet and dry spells during the South Asian summer monsoon season. Nat Clim Chan 4:456–46.1. https://doi.org/10.1038/nclimate2208

Singh S, Ghosh S, Sahana AS, Vittal H, karmakar S (2017) Do dynamic regional models add value to the global model projections of Indian monsoon? Clim Dyn 48:1375–1397

Sinha P, Mohanty UC, Kar SC, Dash SK, Kumari S (2013) Sensitivity of the GCM driven summer monsoon simulations to cumulus parameterization schemes in nested RegCM3. Theor Appl Climatol 112:285–306

Srivastava PK, Han D, Miguel A, Ramirez R, Islam T (2013) Comparative assessment of evapotranspiration derived from NCEP and ECMWF global datasets through Weather Research and Forecasting model. Atmos Sci Let 14:118–125

Sylla MB, Dell'Aquila A, Ruti PM, Giorgi F (2010) Simulation of the intraseasonal and the interannual variability of rainfall over West Africa with a Regional Climate Model (RegCM3) during the monsoon period. Int J Climatol 30:1865–1883

Sylla MB, Giorgi F, Ruti PM, Calmanti S, Dell'Aquila A (2011) The impact of deep convection on the West African summer monsoon climate: a regional climate model sensitivity study. Q J R Meteorol Soc 137:1417–1430

Tawfik AB, Steiner AL (2011) The role of soil ice in land–atmosphere coupling over the United States: a soil moisture precipitation winter feedback mechanism. J Geophys Res 116:D02113

Tugba O, Tufan TT, Turke M, Kurnaz M, Levent M (2016) Projected changes in temperature and precipitation climatology of central asiacordex region 8 by using regcm4.3.5. Atmospheric Research. doi:https://doi.org/10.1016/j.atmosres.2016.09.008

Varikoden H (2006) Dynamic characteristics of atmospheric boundary layer during different phases of monsoon. Department of Atmospheric Sciences Cochin University of Science and Technology, Lakeside Campus, Cochin, India, Doctoral Thesis

VenkataRatnam JK, Kumar K (2005) Sensitivity of the simulated monsoons of 1987 and 1988 to convective parameterization schemes in MM5. J Clim 18:2724–2743

Webster PJ, Magana VO, Palmer TN, Shukla J, Tomas RA, Yanai M, Yasunari T (1998) Monsoons: processses, predictability, and the prospects for prediction. J Geophys Res 103:14451–14510

Wilk MB, Gnanadesikan R (1968) Probability plotting methods for the analysis of data. Biometrika 55(1):1–17